CHAPTER 4

Chapter 4

Peroxoniobium(V) Complexes with Biogenic Co-ligands: Synthesis and Characterization

Contents

New heteroleptic triperoxoniobium complexes with various biogenic ligands have been synthesized from the reaction of sodium tetraperoxoniobate with 30% H_2O_2 and the respective ligand in an aqueous medium. The title compounds have been comprehensively characterized by spectroscopic and other conventional methods including ^{93}Nb NMR and EDX analysis. The density functional theory (DFT) calculation has been performed to verify the feasibility of the proposed structures of the synthesized pNb complexes.

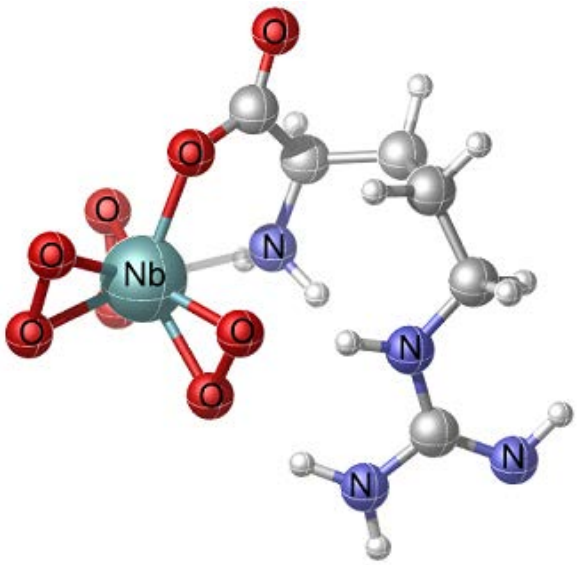

4.1 Introduction

Design and synthesis of water-soluble Nb compounds still remains an exciting challenge for research in inorganic chemistry and a matter of great demand from materials chemistry [1-3], mainly due to the importance of oxides of Nb in diverse fields of advanced technology applications. Utility of pNb compounds as water soluble precursors to obtain Nb-based oxide materials [1-3] and their efficiency as versatile oxidation catalysts [1,4-6] have been well-documented in the literature and adequately highlighted in the Chapter 1. However, the dearth of information on biological activity of pNb compounds [7,8] is indeed conspicuous, since pNb compounds, being water soluble, can be suitable candidates for studying their mode of interaction with biological species. Since the primary focus of the present investigation was to explore some bio-relevant properties of pNb compounds, we have endeavoured to gain an access to pNb derivatives with biogenic species as co-ligands.

An appropriate preference of the co-ligand is a significant prerequisite in order to obtain stable and well-defined peroxometallates. In addition, the coordinating ligand has been demonstrated to have a remarkable effect on the reactivity of peroxometallates (pM) which allowed the activity of pM complexes as stoichiometric or catalytic agents to be modified with ligands [9-12]. A perusal of literature reveals that although tetraperoxo complexes of Nb has been known for over 100 years, there has been continuous attempts to obtain more stable pNb compounds by replacement of one or more peroxo groups with strong ligands [1] such as fluoride [13-19], oxalate [20,21], EDTA [22], citrate [21,23], etc. Although a variety of heteroleptic pNb complexes have been synthesized in recent years [1,20-23], there appears to be a paucity of information regarding well defined synthetic peroxoniobium complexes with coordinated biogenic ligands such as amino acids and other related species [2,24].

In nature, amino acids usually promote solubility of metals in aqueous environment and impart stability by complexation and increase their bioavailability. For the present study we have chosen amino acids *viz.,* L-arginine, L-alanine and L-valine as well as nicotinic acid (also known as niacin) as potential co-ligands to obtain heteroleptic pNb complexes. Amino acids being the primary ligands to interact with a metal in biological systems, a better understanding of the complexation behaviour of Nb with

such ligands is considered to be of vital interest [25-29]. Additionally, transition metal-amino acids complexes have been extensively studied as models for the metal-binding sites in proteins [30]. Most importantly, these ligands possess a carboxylate functional group for easy attachment to the Nb(V) centre in addition to the N-donor site. Carboxylate anions have been known to be excellent co-ligands for stabilizing pNb species [1,31-34].

Among 20 amino acids, arginine is one of the most metabolically multipurpose amino acids [35] with a side-chain guanidino group, which is strongly basic and protonated at different pH values and serves as a biological recognition site *via* hydrogen bonding [36]. Molecular recognition, enzymatic reactions and protein structures are linked with the properties of arginine [37]. It has been demonstrated that arginine is the only substrate for the NO production that affects cardiovascular system (blood vessels and heart) [38]. Arginine functions predominantly as a bidentate ligand, binding metal ions through the α-amino and carboxylate groups. Köse *et* al. [39] recently reported a series of transition metal-arginate complexes with Co(II), Ni(II), Cu(II) and Zn(II). The crystal structure of monoaquabis(arginato-κO,κN)copper(II), $[Cu(arg)_2(H_2O)]NaNO_3$ (**Fig. 4.1**) depicts the coordination of arginate to Cu(II) through α-amino and carboxylate oxygen [39].

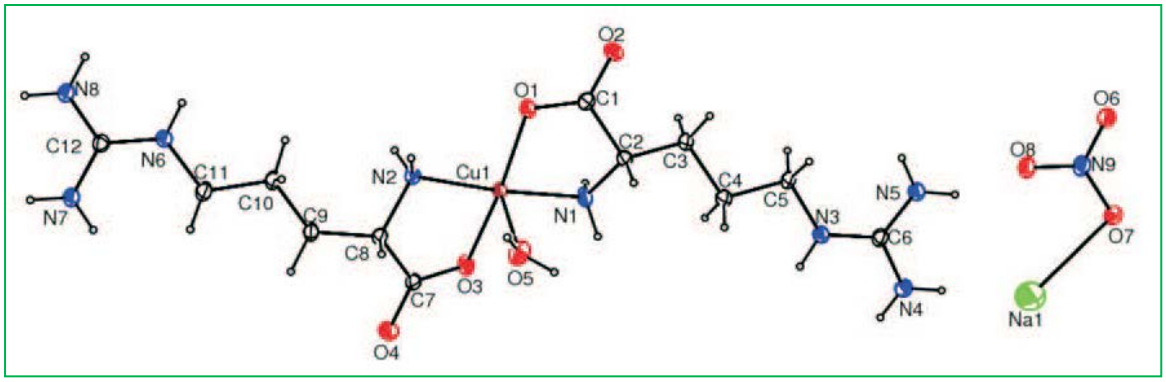

Fig. 4.1 A view of the asymmetric unit of $[Cu(arg)_2(H_2O)]NaNO_3$, showing displacement ellipsoids drawn at the 30% probability level [39].

Apart from the amino acids, pyridine-3-carboxylic acid (nicotinic acid or niacin) is another biologically significant ligand which is an essential vitamin, and it has two potential ligating groups, pyridine ring nitrogen and carboxyl oxygen [40]. Many studies

on biological activities and toxicology have been performed [41,42] with the patented Cr(III)-nicotinato complex, $[(C_6H_4NO_2)_3Cr]^{3+}$ [43]. Recently, Szymanska et *al.* [44] developed a set of oxodiperoxomolybdenum complexes with nicotinic acid coordinated with nicotinic acid N-oxide and protonated nicotinic acid which were found to be active in the oxidation of cyclooctane.

Despite the availability of number of publications, including those from our laboratory, which have dealt with the synthesis and characterization of peroxometal complexes of V [45-53], Mo [54] and W [51,55-57] with amino acid or nicotinic acid as a co-ligand [59], as far as we are aware, the aforementioned ligands have not been used so far to obtain a heteroleptic pNb complex in the solid state.

This chapter describes the synthesis and characterization of heteroleptic peroxoniobium(V) complexes with biogenic co-ligands of the type $Na_2[Nb(O_2)_3L]$ [L = alaninato (**NbAla) (4.1)** or valinato (**NbVal) (4.2**)], $Na_2[Nb(O_2)_3(arg)]\cdot 2H_2O$ [arg = arginate **(NbA**) (**4.3**)], and $Na_2[Nb(O_2)_3(nic)(H_2O)]\cdot H_2O$ [nic = nicotinate **(NbN)** (**4.4**)]. We also report herein the crystal structure of $K_3[Nb(O_2)_4]$ **(KNb)** determined by single crystal X-ray analysis. Although several salts of the tetraperoxoniobate have been characterized structurally, to the best of our knowledge the potassium salt, $K_3[Nb(O_2)_4]$ **(KNb)** has not been reported so far.

4.2 Experimental section

4.2.1 Synthesis of $Na_2[Nb(O_2)_3L]$ [L = alaninato (NbAla) (4.1) or valinato (NbVal) (4.2)]

The precursor molecule $Na_3[Nb(O_2)_4]\cdot 13H_2O$ (**NaNb**) was prepared by following the reported method [6] which is already described in the Chapter 3. In a typical reaction, 0.6550 g (1.25 mmol) of solid sodium tetraperoxoniobate, **NaNb**, was dissolved in minimum volume (4 mL, 35 mmol) of 30% H_2O_2 in a 250 mL beaker. Maintaining the temperature of the reaction solution below 4 °C in an ice bath, the respective amino acid (1.25 mmol) was added gradually to it with constant stirring. The molar ratio of Nb: ligand was maintained at 1:1. The mixture was stirred for *ca.* 15 min till all solid dissolved and a clear solution was obtained, which was subsequently allowed to stand for 3 h at 4 °C. The pH of the resultant solution was recorded to be *ca.* 6.0. On

addition of pre-cooled acetone to the reaction solution with constant stirring, a white pasty product separated out which on repeated treatment with acetone under scratching turned into microcrystalline solid. The compound was separated by centrifugation and dried in *vacuo* over concentrated sulfuric acid.

4.2.2 Synthesis of $Na_2[Nb(O_2)_3(arg)]\cdot 2H_2O$ [arg = arginate (NbA) (4.3)]

Solid $Na_3[Nb(O_2)_4]\cdot 13H_2O$ (0.6550g, 1.25 mmol) was dissolved in 30% H_2O_2 (4 mL, 35 mmol) in a 250 mL beaker in an ice-bath. L-arginine was added to this solution gradually with constant stirring while maintaining the temperature below 4 $^{\circ}$C. At this stage, the pH of the solution was recorded to be *ca.* 8.0. Dilute HNO_3 solution (4 M) was added dropwise to the solution under continuous stirring until the pH was lowered to 6.0. The resulting reaction medium was allowed to stand for 3 h in an ice bath. A white pasty mass separated out on adding pre-cooled acetone to this mixture under vigorous stirring. The mixture was treated repeatedly with acetone under scratching to obtain the microcrystalline product which was separated by centrifugation and finally dried *in vacuo* over concentrated sulfuric acid.

4.2.3 Synthesis of $Na_2[Nb(O_2)_3(nic)(H_2O)]\cdot H_2O$ [nic = nicotinate (NbN) (4.4)]

The procedure consisted of gradual addition of nicotinic acid (1.25 mmol) under constant stirring to a solution of $Na_3[Nb(O_2)_4]\cdot 13H_2O$ (0.6550 g, 1.25 mmol) in 30% H_2O_2 (4 mL, 35 mmol) in an ice-bath. The pH 3 of the reaction solution at this stage was raised to *ca.* 6 by drop wise addition of NaOH solution (8 M). Pre-cooled acetone was added to the solution after allowing it to stand *ca.* 3 h under continuous stirring.The compound was finally obtained as white microcrystalline product by mentioned method under Sections 4.2.1 and 4.2.2, above.

4.2.4 Synthesis of potassium tetraperoxoniobate, $K_3[Nb(O_2)_4]$ (KNb)

Potassium tetraperoxoniobate, $K_3[Nb(O_2)_4]$ was prepared by fusing 2.6 g of KOH with 1 g of Nb_2O_5 in a nickel crucible at 700 °C. After cooling, the solid obtained was dissolved in 100 mL of 1 M aqueous H_2O_2. Unreacted Nb_2O_5 was filtered off and the filtrate was allowed to stand for 24 h at temperature below 4 °C and the colourless

transparent crystals of $K_3[Nb(O_2)_4]$ were obtained from the solution from which a suitable crystal for single crystal X-ray structure determination was collected.

4.2.5 Elemental analysis

Quantitative determination of niobium, peroxide, carbon, hydrogen, nitrogen and sodium were accomplished by methods described in Chapter 2. The analytical data of the compounds are presented in **Table 4.1**.

4.2.6 Physical and spectroscopic measurements

The compounds were characterized according to the described methods in Chapter 2, with the help of spectroscopic measurements, thermogravimetric analysis as well EDX analysis. **Table 4.2** summarizes the structurally significant IR and Raman bands along with their assignments. ^{1}H and ^{13}C NMR chemical shift values of the complexes are represented in the **Tables 4.3** and **4.4** and spectra are presented in **Fig. 4.5**-**4.21**. ^{93}Nb NMR spectra for the complexes are presented in **Fig. 4.22**. TGA of the complexes are represented in the **Fig. 4.23**-**4.27**.

4.2.7 Computational details

The Gaussian09 programme [59] at the B3LYP/LANL2DZ level of theory has been used to perform density functional theory (DFT) [60] calculations. The ground-state geometry of the synthesized niobium complexes were obtained in the gas phase and the minima of the optimized structures were verified by the absence of imaginary frequencies.

4.3 Results and discussion

4.3.1 Synthesis

A reasonably straightforward synthetic route has been established to obtain stable and water soluble pNb complexes **4.1**-**4.4** in a ligand sphere of niacin or amino acids *viz.,* alanine, valine or arginine as co-ligand. The procedure is based on the reaction of sodium tetraperoxoniobate, $Na_3[Nb(O_2)_4]\cdot 13H_2O$ with 30% H_2O_2 and the respective co-ligand,

in an aqueous medium at near neutral pH. The maintenance of pH of *ca.* 6.0 apparently favoured the formation of the triperoxoNb species and co-ordination of the organic ligands in their anionic form, facilitating its stabilization and leading to the synthesis of the desired complexes. The procedure included other requirements such as maintenance of temperature at ≤ 4 °C and limiting water to that contributed by 30% H_2O_2. Despite many attempts, it was not possible to obtain crystals of the developed compounds large enough for an X-ray crystal structure. The crystals of the homoleptic potassium tetraperoxoniobium complex $K_3[Nb(O_2)_4]$ (**KNb**) were prepared by adopting a procedure which is a modification of the reported method for synthesis of microcrystalline **KNb** [6,61-63]. The compounds were observed to be stable in the solid state for several weeks when stored dry in closed container at < 30 °C.

4.3.2 Characterization

The elemental analysis data (**Table 4.1**) for each of the title compounds, *viz.*, **NbAla (4.1)**, **NbVal (4.2), NbA (4.3)** and **NbN (4.4)**, indicated the presence of three peroxide groups and one ancillary ligand. For the **KNb** complex, the $Nb:O_2^{2-}$ ratio was found to be 1:4 as expected for a tetraperoxoniobium species. Energy-dispersive X-ray (EDX) spectroscopic analysis clearly showed the presence of Nb, Na, C, N and O in the complexes **4.1-4.4**. The obtained data on the composition of the compounds from EDX analysis were in good agreement with elemental analysis values (**Table 4.1**). The compounds were diamagnetic in nature as was evident from the magnetic susceptibility measurements, in conformity with the presence of Nb in its +5 oxidation state.

4.3.2.1 The IR and Raman spectra of the compounds

The title compounds **4.1-4.4** displayed a distinctive spectral pattern in the IR region. The Raman spectra of the compounds complemented the IR spectra, confirming the presence of co-ordinated peroxo and the respective co-ligand in each of them. The significant general features of IR and Raman spectra are summed up in **Table 4.2**. The spectra for the complexes are presented in **Fig. 4.2**-**Fig. 4.10**.

Table 4.1 Analytical data for the synthesized peroxoniobium complexes

Compounds	% found from elemental analysis/EDX (Theoretical %)					% O_2^{2-} content (Theoretical %)	Ratio of Nb:O_2^{2-}
	C	H	N	Nb[a]	Na		
NbAla	11.03	1.84	4.28	28.59	14.19	29.42	1:2.97
	(11.15)	(1.86)	(4.33)	(28.77)	(14.25)	(29.72)	
NbVal	17.23	2.87	4.01	26.37	13.19	27.31	1:3.04
	(17.10)	(2.85)	(3.99)	(26.48)	(13.11)	(27.36)	
NbA	16.29	3.76	12.46	21.01[a]	11.14	21.71	1:3
	16.15		12.76	20.84	10.47		
	(16.21)	(3.83)	(12.61)	(20.92)	(10.36)	(21.61)	
NbN	18.41	1.99	3.55	23.52[a]	11.63	24.54	1:3.03
	18.37		3.61	23.57	11.66		
	(18.32)	(2.03)	(3.56)	(23.64)	(11.70)	(24.43)	
KNb				27.13	-	37.22	1:3.98
				(27.47)		(37.85)	

[a]Determined by AAS.

A triperoxo niobium species with triangularly bonded peroxo group has been reported to exhibit a diagnostic IR pattern with three ν(O-O) bands in the 800-880 cm^{-1} region [1,64]. The IR and Raman spectra of each of the compounds **4.1**-**4.4** enabled clear identification of three sharp absorptions representing the characteristic ν(O-O) modes of peroxo group, in addition to the ν_{as}(Nb-O_2) and ν_s(Nb-O_2) vibrations, as has been expected, in the 870-810 and 500-600 cm^{-1} region, respectively [1,64]. On the other hand, the IR spectrum of **KNb**, in agreement with the previous reports on other tetraperoxNb complexes, showed a single peak for O-O stretching at 815 cm^{-1} apart from the ν_{as}(Nb-O_2) and ν_s(Nb-O_2) at 599 and 542 cm^{-1}, respectively **(Fig. 4.2)** [65].

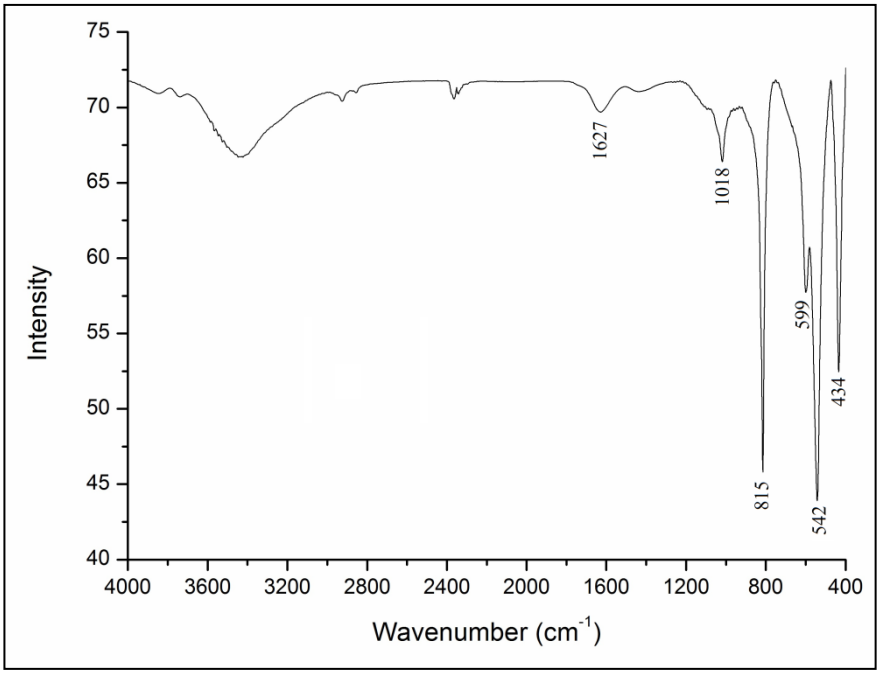

Fig. 4.2 IR spectrum of **KNb**.

On the basis of the available reported data pertaining to metal compounds with co-ordinated amino acid and nicotinic acid as ligands, empirical assignments could be derived for the IR and Raman bands observed for the title compounds [66-72]. The free alanine spectrum exhibited $\nu_{as}(COO^-)$ and $\nu_s(COO^-)$ vibrations at 1586 and 1409 cm^{-1}, respectively with a frequency difference $\Delta\nu$ = 177 cm^{-1} [$\Delta\nu = \nu_{as}(COO^-)-\nu_s(COO^-)$] (**Fig. 4.3**). In case of free valine, these bands were located at 1570 and 1395 cm^{-1} (**Fig. 4.5**). A definite shift of $\nu_{as}(COO^-)$ to a higher frequency and that of $\nu_s(COO^-)$ to a lower frequency (**Table 4.2**) and the resulting frequency difference of 266 and 234 cm^{-1} found in **NbAla (4.1)** and **NbVal (4.2)**, respectively, are typical of unidentately co-ordinated

non-protonated carboxylate groups (**Table 4.2**) [66,67]. The participation of amino groups of the ligands in co-ordination was indicated by the shift of *v*(NH) frequencies to a lower wave number in comparison to the free amino acid bands. The well-resolved medium intensity band observed in the spectra of **NbAla (4.1)** at 3081 cm^{-1} and the two bands occurring at 3058 and 3162 cm^{-1} for **NbVal (4.2)** have been ascribed to the NH stretchings of co-ordinated amino acid [66]. The $\delta(NH_2)$ vibrations appeared at *ca.* 1510 cm^{-1} in the spectra of both the complexes. A band at 490 cm^{-1} has been observed in the free alanine zwitterion for NH_3^+ torsion [73]. On complexation, the peak disappeared and additional peaks have been obtained at 477 and 411 cm^{-1} in the IR spectrum of **NbAla (4.1)** which may be assigned to ν_{as}(Nb-N) and ν_s(Nb-N) stretchings, respectively [66]. Similarly, the presence of 430 and 405 cm^{-1} peaks owing to ν_{as}(Nb-N) and ν_s(Nb-N) stretchings in the spectrum of **NbVal (4.2)** constitutes an additional valuable indication for the involvement of NH_2 group in coordination [66]. The intense peak observed between 2980-2880 cm^{-1} in the Raman spectra occurring as a medium intensity peak in the IR spectra of both the complexes have been assigned to C-H stretching vibration.

The IR spectra of arginine, as well as of arginato-metal complexes have been reported previously [73-75]. In the spectrum of free arginine $\nu_{as}(COO^-)$ and $\nu_s(COO^-)$ modes are observed at 1606 and 1425 cm^{-1}, respectively with $\Delta\nu = 181$ [$\Delta\nu = \nu_{as}(COO^-) - \nu_s(COO^-)$]; whereas, in the case of the complex **NbA (4.3) (Fig. 4.7)**, the corresponding absorptions appeared at 1636 cm^{-1} and 1406 cm^{-1}, respectively. The shift of $\nu_{as}(COO^-)$ to higher frequency and that of $\nu_s(COO^-)$ to a lower frequency compared to the free ligand values, with an increase in the $\Delta\nu$ (= 230 cm^{-1}), is typical of unidentate co-ordination of carboxylate group [66].

In the Raman spectrum of the **NbA** compound, weak intensity bands representing $\nu_{as}(COO^-)$ and $\nu_s(COO^-)$ vibrations have been located at 1630 and 1410 cm^{-1}, respectively. The *v*(C-H) occurred as an intense peak at 2934 cm^{-1} in the Raman spectrum in contrast to its presence as a weak band in the IR. Two bands typical of $\nu(NH_2)$ are observed at 3352 and 3288 cm^{-1} in the free ligand spectrum [73]. A new peak appeared at 3193 cm^{-1} in the spectrum of the complex **NbA (4.3)** indicative of co-ordinated amino group [73]. However, the other absorptions representing *v*(N-H) could not be assigned with certainty owing to their overlapping with *v*(OH) modes of lattice water, appearing as a broad band in the 3500-3300 cm^{-1} region.

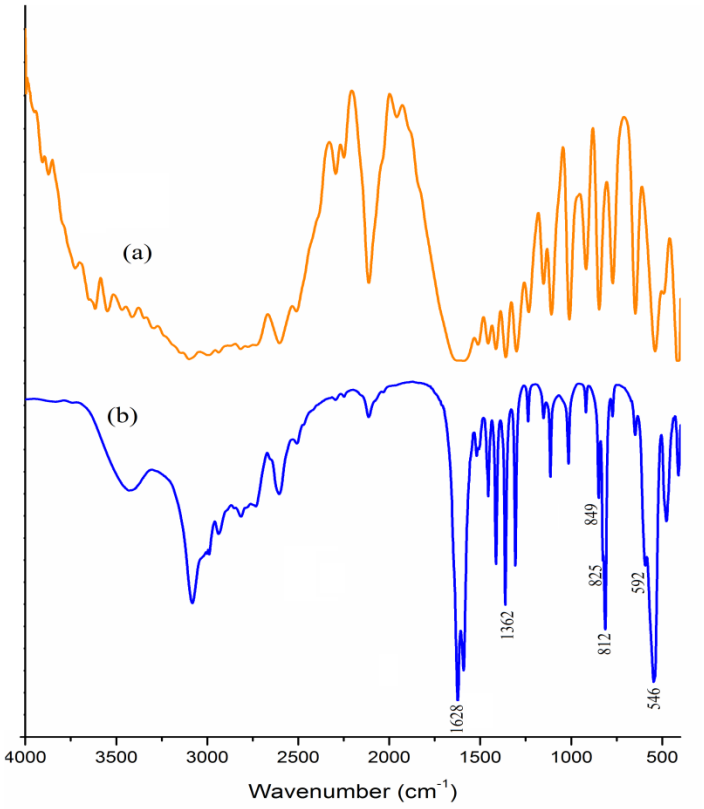

Fig. 4.3 IR spectra of (a) alanine and (b) **NbAla**.

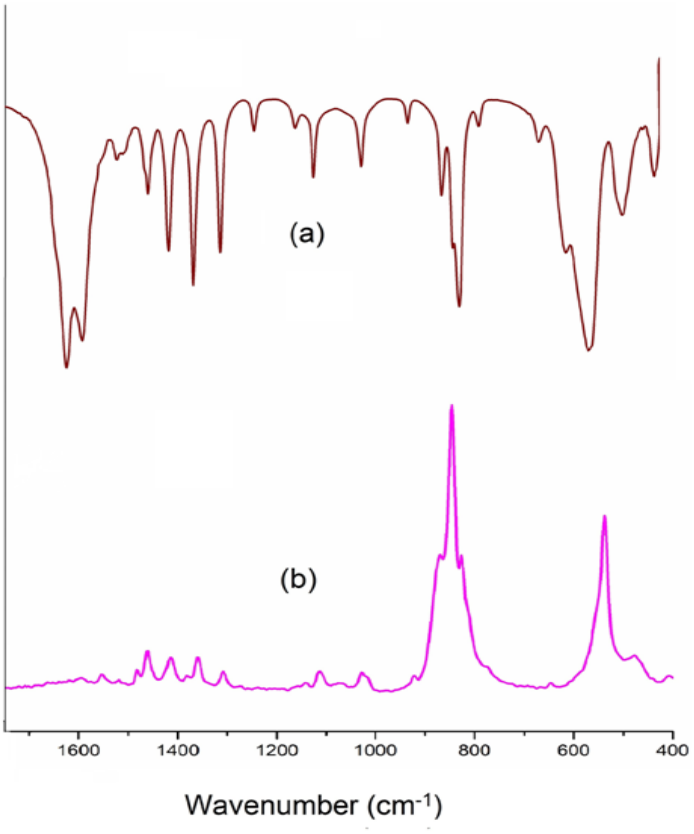

Fig. 4.4 (a) IR & (b) Raman spectra of **NbAla**.

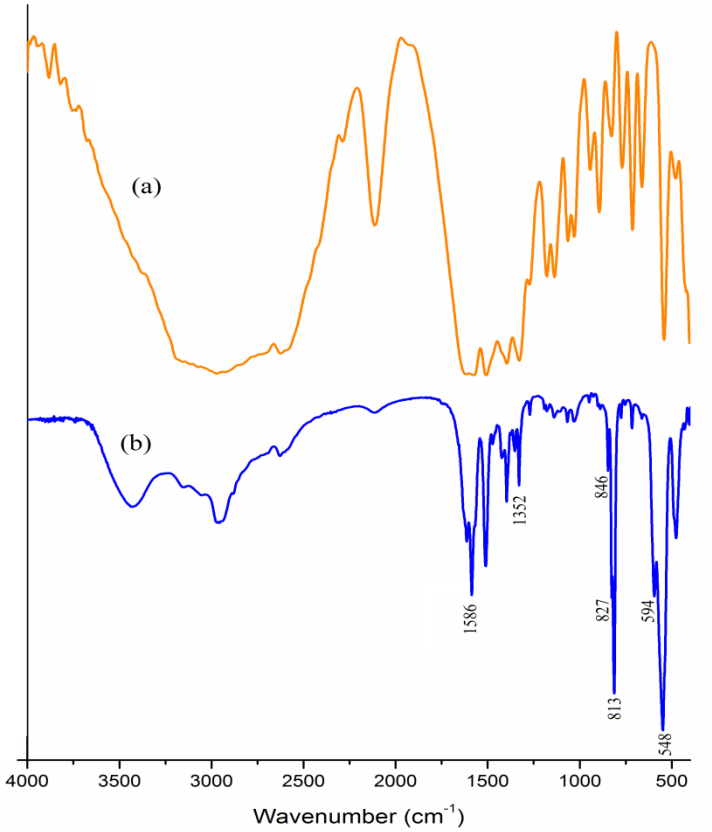

Fig. 4.5 IR spectra of (a) valine and (b) **NbVal**.

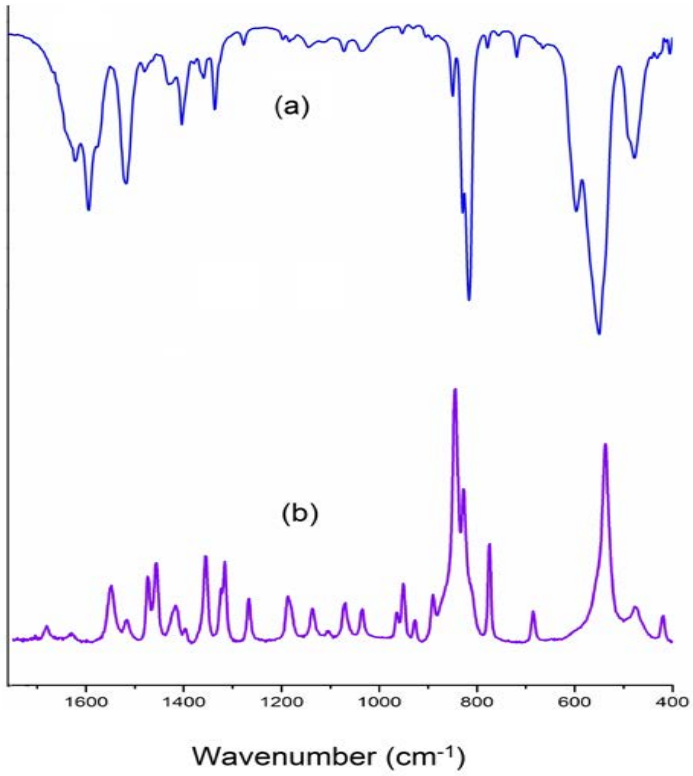

Fig. 4.6 (a) IR & (b) Raman spectra of **NbVal**.

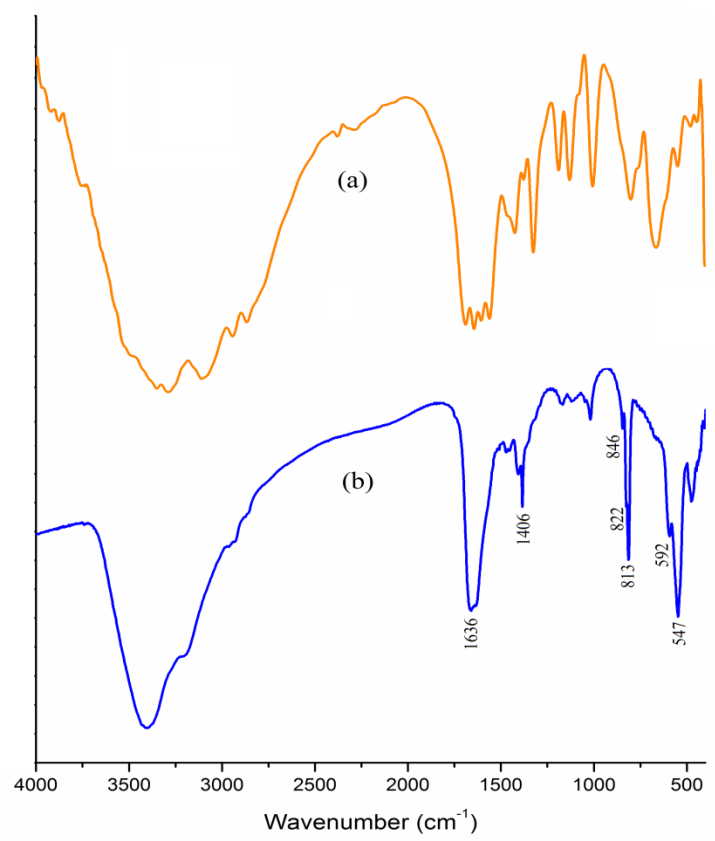

Fig. 4.7 IR spectra of (a) arginine and (b) **NbA**.

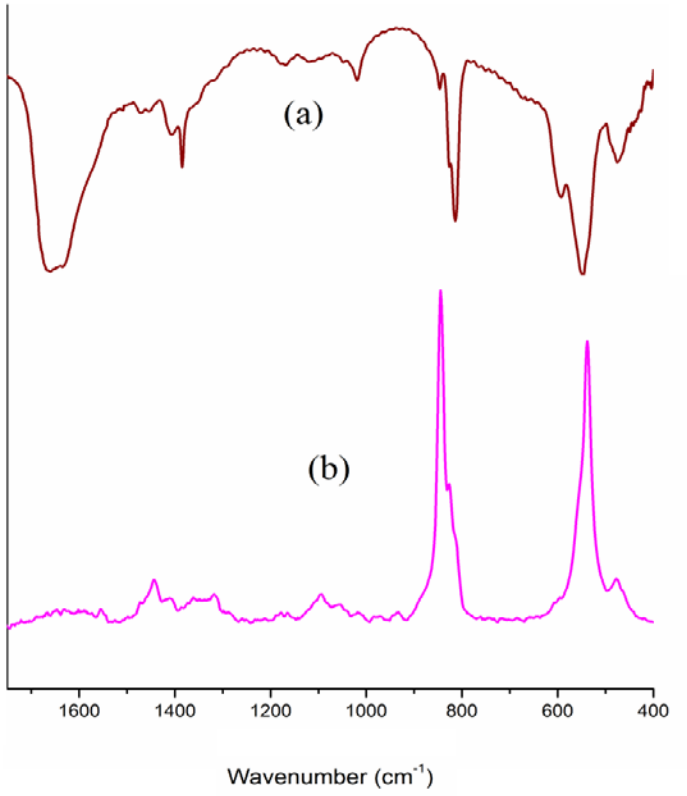

Fig. 4.8 (a) IR & (b) Raman spectra of **NbA.**

For the compound **NbN (4.4)** (**Fig. 4.9** and **Fig. 4.10**), the presence of carboxylato bonded nicotinic acid has been clearly demonstrated by its IR and Raman spectra (**Table 4.2**). A number of reports are available on IR spectral characterization of metal complexes containing co-ordinated nicotinic acid [69-72]. Moreover, the IR and Raman spectra of nicotinic acid have been thoroughly investigated by Kumar and Yadav [70]. Solid sodium nicotinate exhibits major carboxylate IR bands at 1620 and 1416 cm^{-1}, respectively, for $\nu_{as}(COO^-)$ and $\nu_s(COO^-)$ [72]. The positions of $\nu_{as}(COO^-)$ and $\nu_s(COO^-)$ stretchings in both IR and Raman spectra of **NbN (4.4)** and the corresponding $\Delta\nu$ (=237 cm^{-1}) value provide clear evidence of unidentate co-ordination of a non-protonated carboxylato group to the metal atom. **NbN (4.4)** also shows the presence of three peroxo groups side-on bounded to niobium metal which is evidence from **Fig. 4.9** and **Fig. 4.10**.

Furthermore, a significantly less intense aromatic *v*(CC) band at 1568 cm^{-1} depicts monodentate coordination of a carboxylate group to Nb [58]. Since the *v*(CC) mode, *v*(CN) absorption as well as pyridine ring vibrations at 1476, 1016 and 940 cm^{-1}, respectively, do not undergo any positive shift relative to the respective free ligand values, coordination *via* pyridine ring nitrogen can safely be ruled out [69]. The presence of water molecule in the complex was apparent from the observance of broad and intense *v*(OH) bands in the 3500 to 3400 cm^{-1} region. Further confirmation for the presence of co-ordinated water in the compound was obtained from the consistent appearance of a moderate intensity signal at 769 cm^{-1} attributable to rocking mode of water [76]. The intense band appearing at 3077 cm^{-1} in the Raman spectrum has been ascribed to *v*(CH) vibration.

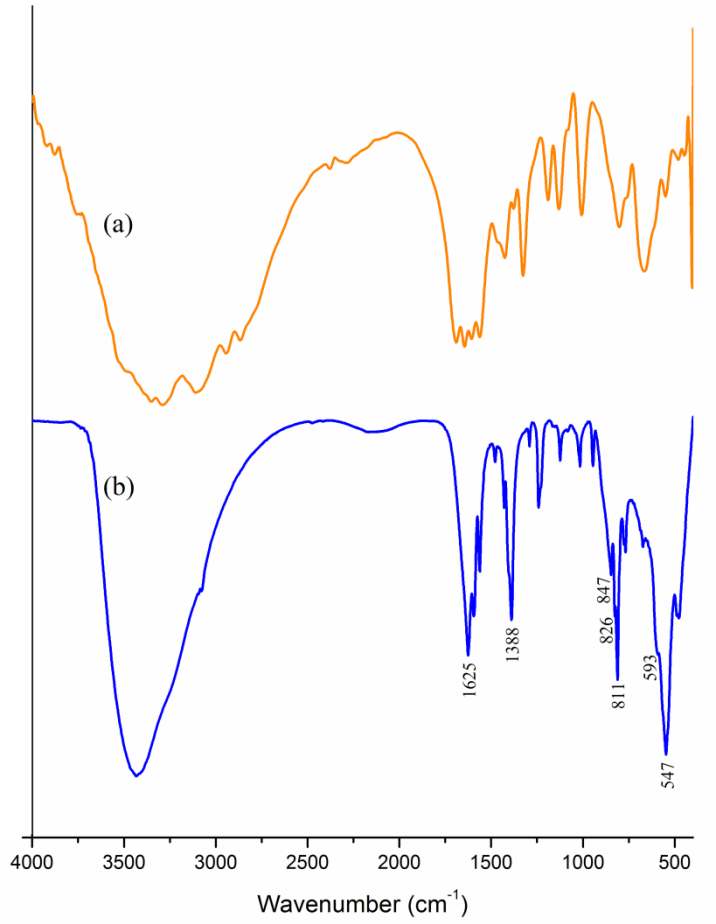

Fig. 4.9 IR spectra of (a) nicotinic acid and (b) **NbN**.

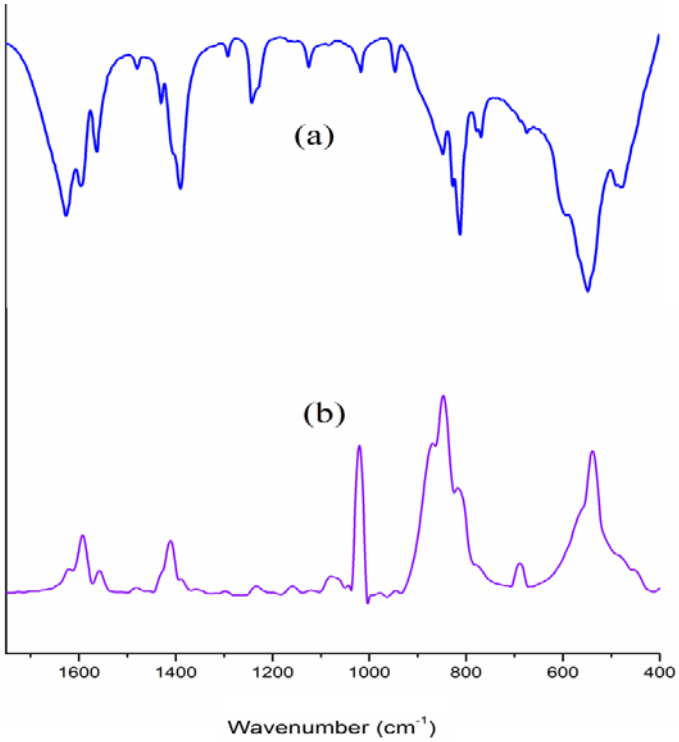

Fig. 4.10 (a) IR & (b) Raman spectra of **NbN**.

Table 4.2 Experimental and theoretical infrared and Raman spectral data (in cm^{-1}) for the compounds, **NbAla**, **NbVal**, **NbA** and **NbN**[a]

Assignment			**NbAla**	**NbVal**	**NbA**	**NbN**
ν(O-O)	IR	Exp.	849(m), 825(sh), 812(s)	846(m), 827(sh), 813(s)	846(m),822(sh), 813(s)	847(m), 826(sh), 811(s)
		Calc.	864, 823, 811	858, 775	837, 865, 889	807, 872
	R	Exp.	868(sh), 845(s), 826(sh)	889(sh), 845 (s), 827(sh)	857(sh), 847(s), 823(sh)	867(sh), 847(s), 817(sh)
		Calc.	872, 824	878, 851, 815	806, 853, 879	813, 828, 876
ν_s(Nb-O_2)	IR	Exp.	546(s)	548(s)	547(s)	547(s)
		Calc.	550	544	528	523
	R	Exp.	537(s)	536(s)	538(s)	542(s)
		Calc.	551	528	528	554
ν_{as}(Nb-O_2)	IR	Exp.	592(m)	594(m)	592(m)	593(sh)
		Calc.	692	651	604	605
	R	Exp.	645(sh)	684(sh)	567(sh)	571(sh)
		Calc.	692	678	575	598
ν_{as}(COO^-)	IR	Exp.	1628(s)	1586 (s)	1636(s)	1625(s)
		Calc.	1666	1601	1615	1649
	R	Exp.	1619(vw)	1629(vw)	1630(vw)	1627(sh)
		Calc.	1665	1600	1609	1627
ν_s(COO^-)	IR	Exp.	1362(m)	1352(m)	1406(m)	1388(s)
		Calc.	1405	1310	1375	1378
	R	Exp.	1414(vw)	1393(vw)	1410(vw)	1393(sh)
		Calc.	1388	1369	1403	1335

[a]s, strong; m, medium; vw, very weak; sh, shoulder.

4.3.2.2 ^{1}H, ^{13}C and ^{93}Nb NMR studies

In **Tables 4.3** and **4.4**, relevant ^{1}H and ^{13}C NMR resonances for the complexes are listed along with those of the free ligand for comparison. Crucial structural information regarding the complexes, including the co-ordination mode of the ligand to the Nb atom, as well as their stability in solution have been gathered from the complete analysis of the NMR spectra. The major NMR resonances were interpreted according to available literature data. The ^{1}H-NMR spectra in D_2O have shown the expected integration and peak multiplicities [**Fig. 4.11-Fig. 4.14**].

The ^{1}H NMR spectra for the pNb complexes **NbAla (4.1)** and **NbVal (4.2)** in D_2O are presented in **Fig. 4.11** and **Fig. 4.12**, respectively, and the corresponding chemical shifts for the complexes and free amino acids are listed in **Table 4.3**. A close resemblance was observed in the ^{1}H NMR spectra of the complexes and the spectra of the respective amino acid displaying the well-resolved resonances with expected integration and peak multiplicities. The spectra however, showed distinct up field shift of the proton signals attached to carbon atoms C-2 and C-3 relative to the free ligand, consistent with the occurrence of metal ligand co-ordination [37,77]. Similar observations were made previously in cases of metal compounds containing complexed amino acid [37,77,78]. The position of H-4 and H-5 protons in **NbVal (4.2)** remains practically unaffected which may not be unexpected as these atoms are well-separated from the actual ligand donor sites. The spectral pattern of the pNb complex with arginine as co-ligand displayed 4 major peaks, as has been observed in the spectrum of the free arginine [37]. The spectrum of the **NbA (4.3)** (**Fig. 4.13**) complex showed upfield shift of all the resonances relative to the free ligand indicating co-ordination of the ligand to the metal centre [37,77].

The ^{1}H spectra of nicotinic acid in D_2O has been studied and reported by Khan and co-workers [79] under varying pH conditions. A ^{1}H NMR pattern typical of a nicotinate anion was observed with four well-resolved resonances in the spectrum of the compound **NbN (4.4)** [79]. As expected for nicotinate anion, the spectrum showed characteristic up field shift of each of the four resonances corresponding to the aromatic protons H(2) to H(6) (**Fig. 4.14**), relative to the zwitterionic free ligand values [77].

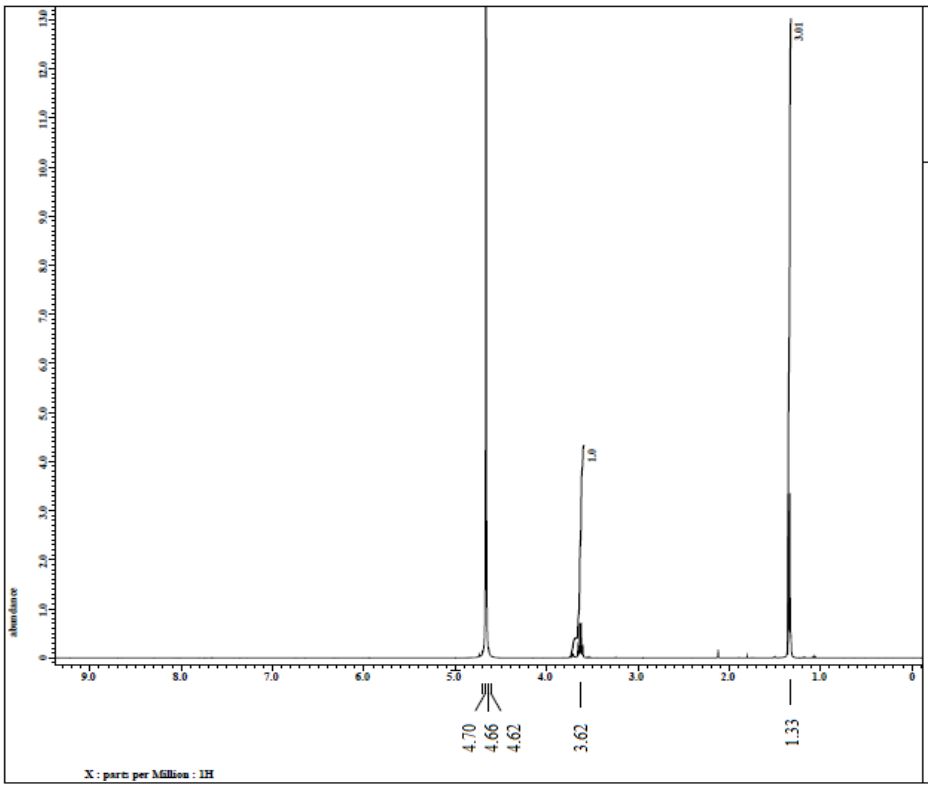

Fig. 4.11 ^{1}H NMR spectrum of **NbAla** in D_2O.

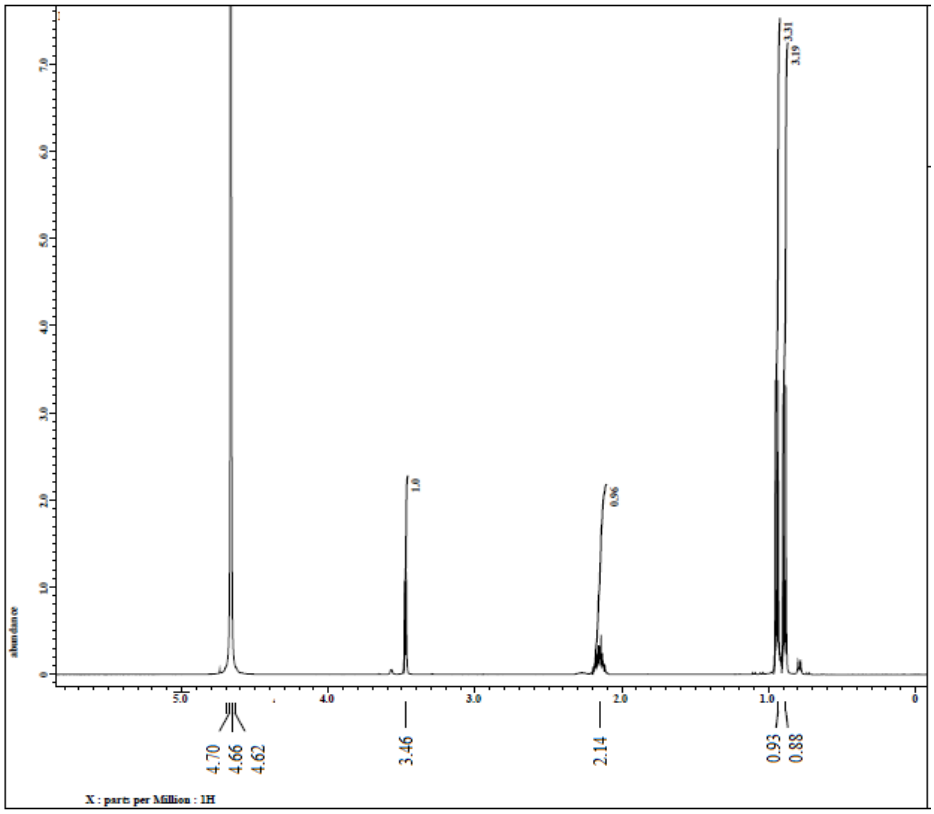

Fig. 4.12 ^{1}H NMR spectrum of **NbVal** in D_2O.

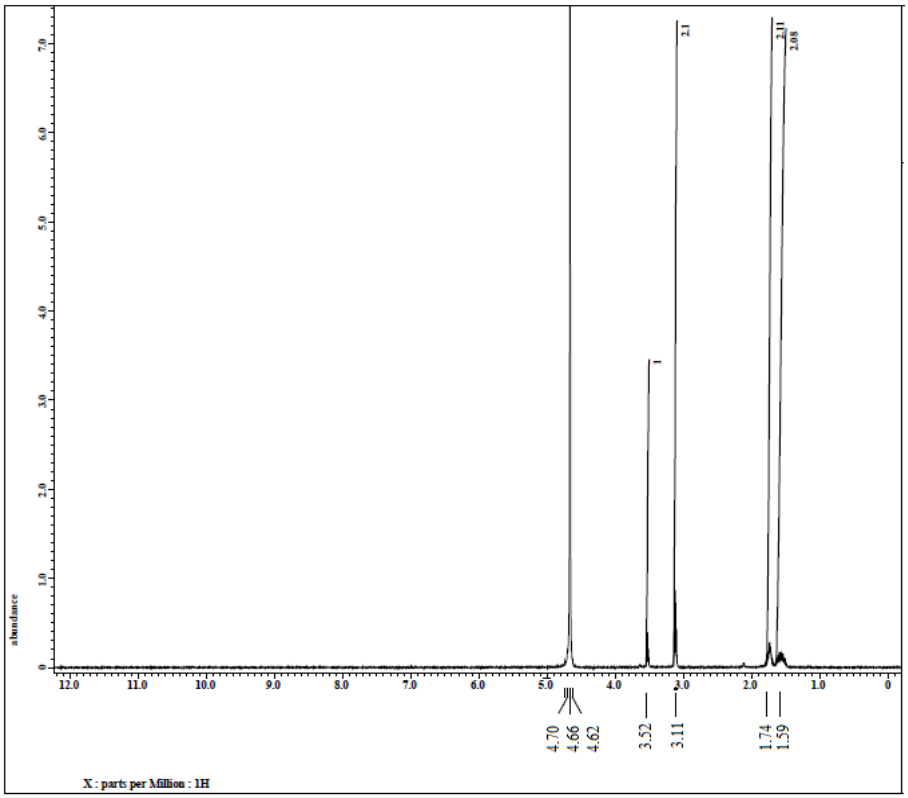

Fig. 4.13 ^{1}H NMR spectrum of **NbA** in D_2O.

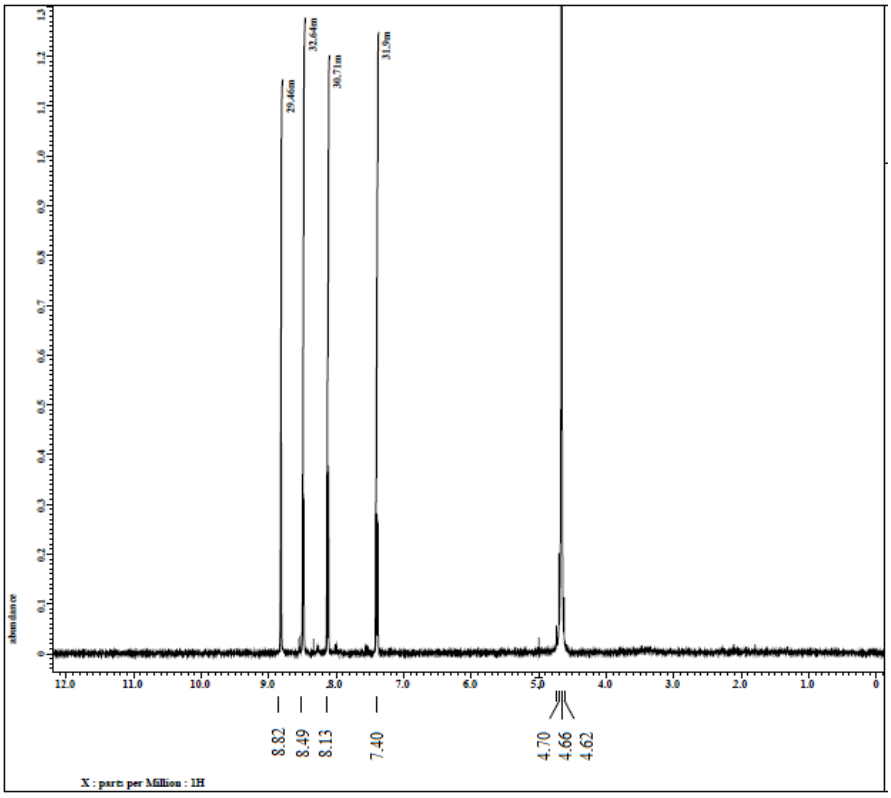

Fig. 4.14 ^{1}H NMR spectrum of **NbN** in D_2O.

Table 4.3 ^{1}H NMR chemical shifts for ligands and heteroligand peroxo-niobate complexes

Compound	Chemical shift (ppm)[a]				
	H-2	H-3	H-4	H-5	H-6
Alanine	3.68	1.35			-
NbAla	3.62	1.33			-
Valine	3.48	2.15	0.93	0.88	-
NbVal	3.46	2.14	0.93	0.88	-
Arginine	3.76	1.89	1.66	3.23	-
NbA	3.52	1.74	1.59	3.11	-
Nicotinic acid	8.97	-	8.68	7.93	8.76
NbN	8.82	-	8.13	7.40	8.49

[a]See **Fig. 4.25** for the atomic numbering.

The ^{13}C chemical shift induced by coordination has been widely utilized as a convenient means to understand bonding pattern of ancillary ligands in peroxo-metal complexes [80-82]. The ^{13}C NMR spectra of ligands alanine and valine exhibited resonances due to the carboxylate carbon atoms at 175.81 and 174.24 ppm, respectively, apart from the expected peaks corresponding to the side chain carbon atoms [37]. As seen in **Fig. 4.15**, **Fig. 4.16** and **Table 4.4**, all the signals appear with downfield shift to varying degrees, *vis-a-vis* the free amino acids, obviously resulting from the deshielding of carbon atoms as a consequence of complexation [37,83,84]. The most significant co-ordination induced shift $\Delta\delta$ (δ_{complex} -$\delta_{\text{free carboxylate}}$) ≈ 7.02 ppm for **NbAla (4.1)** [8.55 ppm for **NbVal (4.2**)] occurred as expected for the metal linked carboxylate carbon, suggesting metal-ligand interaction [83,84].

The ^{13}C NMR spectrum of the free arginine in D_2O, displays typical resonance for carboxylate carbon atom at 183.17 ppm, in addition to the five other well resolved peaks corresponding to carbon atoms C(2) to C(6) [26]. The spectrum of **NbA (4.3)** (**Fig. 4.17**), on the other hand displayed the carboxylate resonance at lower field of 215.45 ppm thus testifying to the existence of complexed carboxylate group [37,83,84]. The substantial downfield shift relative to free carboxylate, with $\Delta\delta \approx 32$ ppm, indicated strong metal-ligand interaction as has been reported earlier in cases of some other peroxo metal carboxylate complexes [83,84]. The guanidyl C resonance along with the

resonances of alkyl groups (C-5 and C-4) showed very little shift, whereas the resonances of α-CH and β-CH_2 groups are shifted to higher field by *ca.*1 ppm. These results indicated the co-ordination of carboxylate and amino groups of the ligand to the niobium centre and are consistent with observations made in cases of other reported arginine containing metal compounds [37].

For the compound **NbN (4.4)**, the ^{13}C spectrum provided further persuasive evidence in support of the presence of nicotinate anion in it (**Fig. 4.18**) by displaying resonances for ring carbon atoms in the region expected for nicotinate anion [79]. The peak attributable to metal bound carboxylate carbon, as in the case of **NbA (4.3)**, appeared at a considerably lower field of 210.78 ppm, compared to the carboxylate resonance of the free nicotinic acid [83,84]. Appearance of carboxylate carbon resonance as a single peak in the spectra of the compounds **4.1**-**4.4**, reflected a single carbon environment for co-ordinated carboxylate [83,84]. Thus the results of the NMR analysis evidenced for the presence of only one complex species in solution in each case. It is therefore apparent that the title compounds did not hydrolyze in solution.

Table 4.4 ^{13}C NMR chemical shift for ligands and the developed triperoxoniobium complexes

Compound	Carboxylate Carbon	Chemical Shift (ppm)[a]				
		C_2	C_3	C_4	C_5	C_6
Alanine	175.81	50.55	16.19			
NbAla	182.83	51.26	19.50			
Valine	174.24	60.34	29.07	17.96	16.63	
NbVal	182.79	61.84	31.67	19.02	16.75	
Arginine	183.17	55.59	31.64	24.51	41.02	156.81
NbA	215.45	54.59	30.28	23.99	40.64	156.83
Nicotinic acid	168.25	143.04	135.49	142.49	126.94	145.89
NbN	210.78	149.06	137.69	142.46	128.76	150.51

[a]See **Fig. 4.25** for the atomic numbering

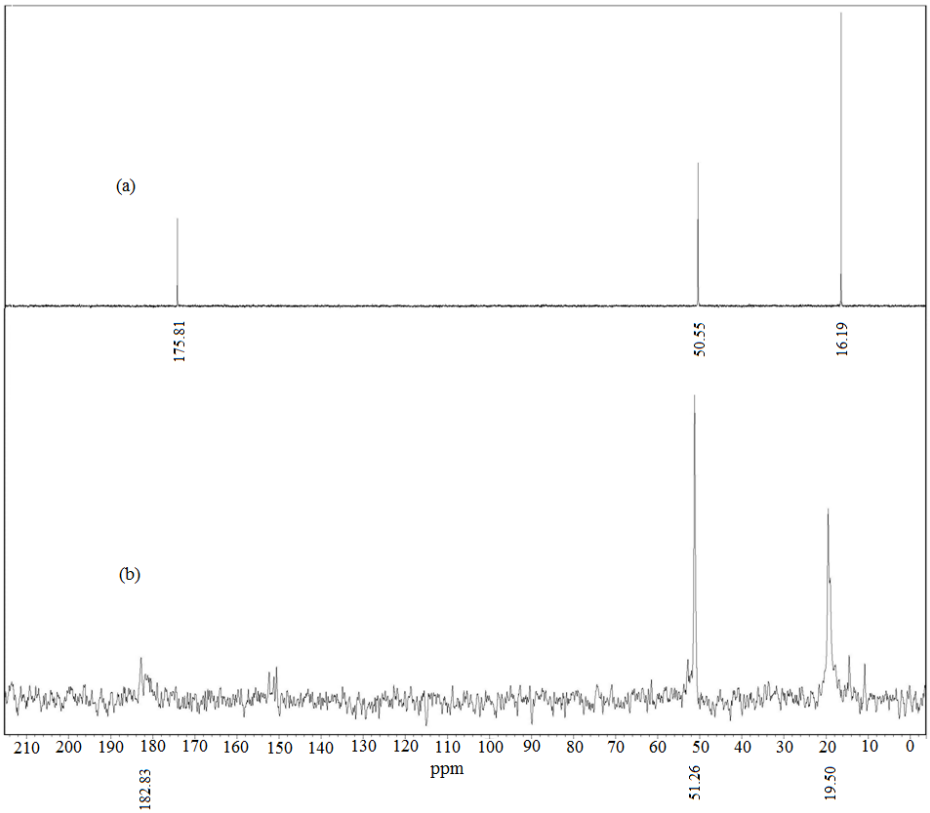

Fig. 4.15 ^{13}C NMR spectra of (a) alanine and (b) **NbAla** in D_2O.

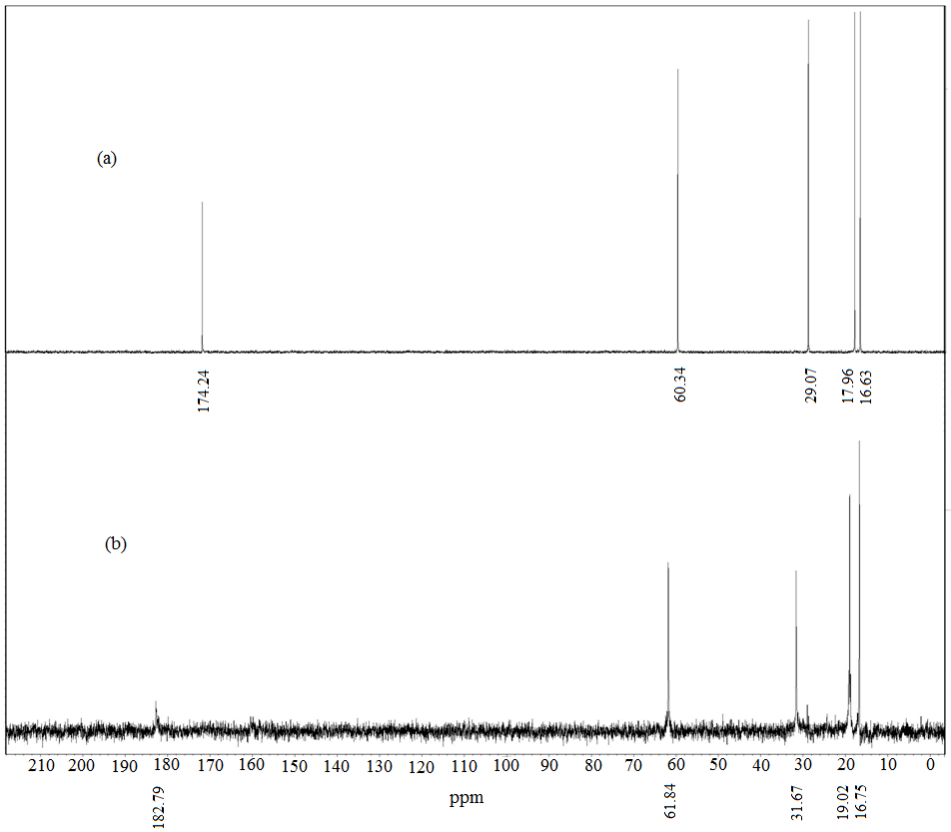

Fig. 4.16 ^{13}C NMR spectra of (a) valine and (b) **NbVal** in D_2O.

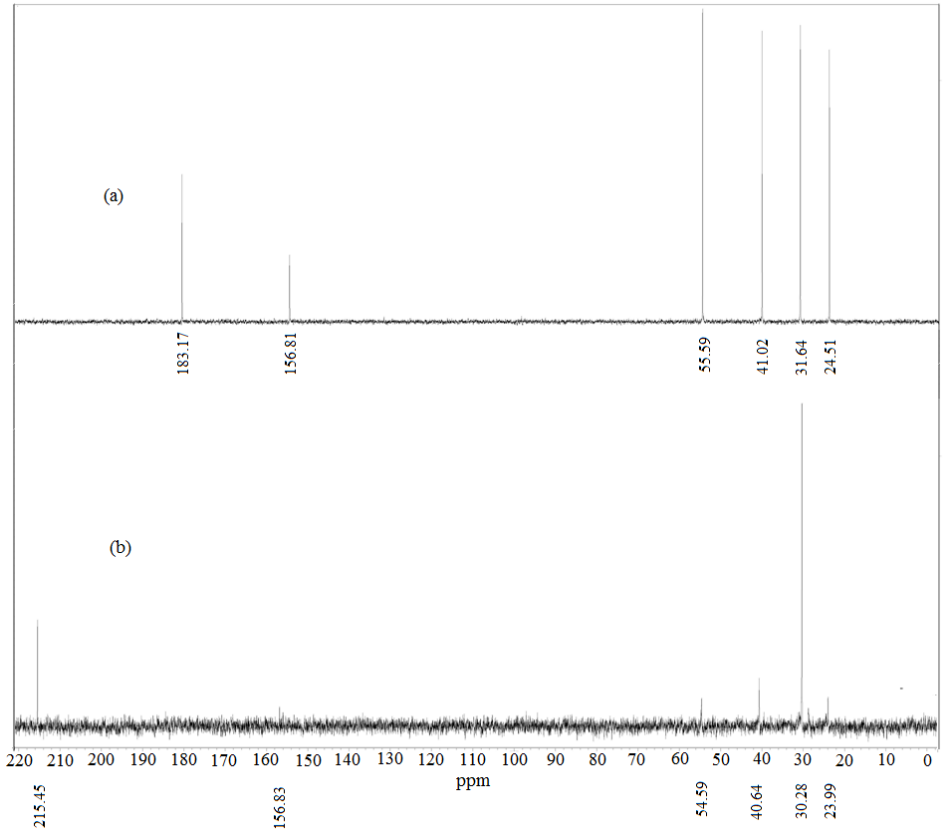

Fig. 4.17 ^{13}C NMR spectra of (a) arginine and (b) **NbA** in D_2O.

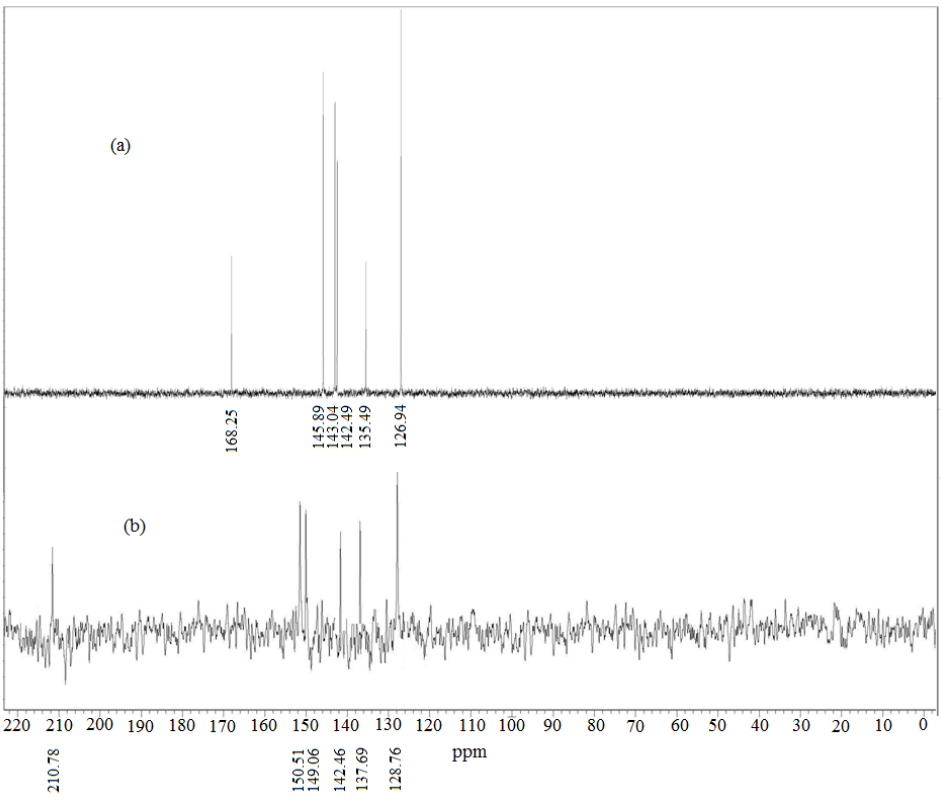

Fig. 4.18 ^{13}C NMR spectra of (a) nicotinic acid and (b) **NbN** in D_2O.

In the ^{93}Nb NMR spectrum of each of the synthesized triperoxoniobium complexes, a single resonance at -1529, -1528, -1537 and -1526 ppm were observed for **NbAla (4.1)**, **NbVal (4.2)**, **NbA (4.3)** and **NbN (4.4)**, respectively, (**Fig. 4.19b-4.19e**) which resembled closely the spectra of polymer anchored triperoxoniobium complexes **3.1** and **3.2**. Slight shifting of peak positions may be ascribed to the presence of different ancillary ligands in the complexes. On the other hand, the ^{93}Nb NMR spectrum of **KNb** displays a peak at -1483 ppm (**Fig. 4.19a**), which compared well with the spectrum of sodium tetraperoxoniobate species, **NaNb** (**Fig. 3.11a**). Thus the ^{93}Nb NMR data for the complexes **4.**1-**4.4** indicated eight co-ordinated environment for Nb in each of the complexes, as has been observed in the cases of macro complexes, **3.1** and **3.2**.

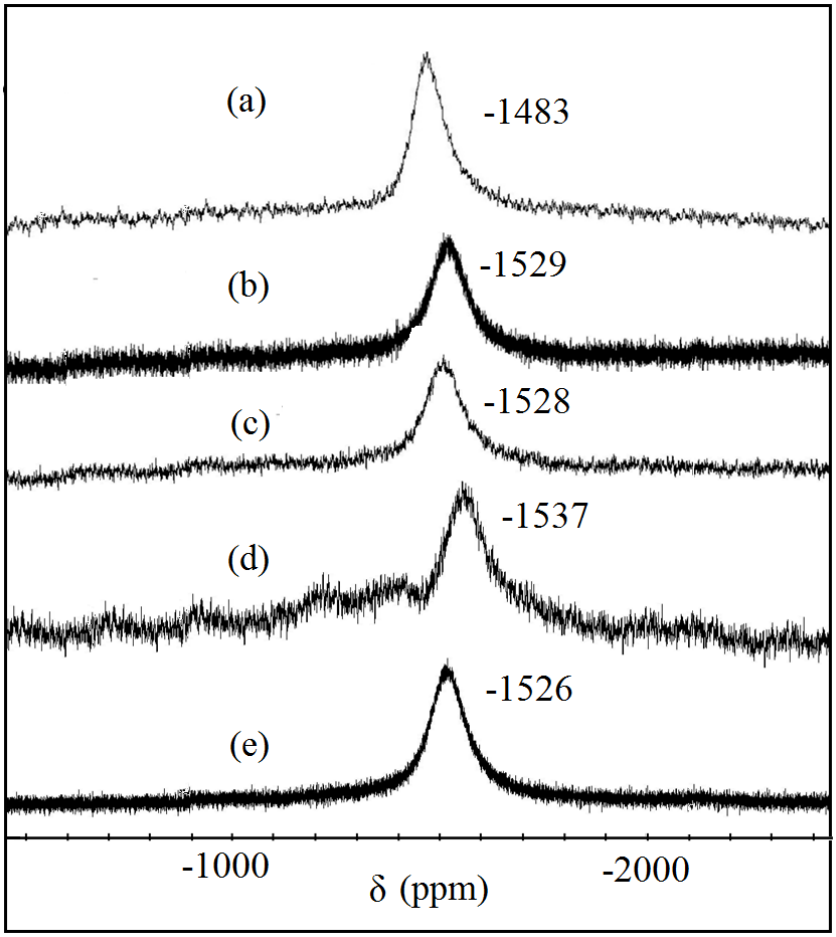

Fig. 4.19 ^{93}Nb NMR spectra of (a) **KNb**, (b) **NbAla (4.1)**, (c) **NbVal (4.2)**, (d) **NbA (4.3)** and (e) **NbN (4.4)** in D_2O.

4.3.2.3 Thermal analysis

The TGA-DTG plots [**Fig. 4.20-Fig. 4.24**] obtained for the title compounds on heating up to a temperature of 700 ^{o}C, revealed a close analogy among their decomposition patterns. Each of the compounds, as has been observed in case of previously reported complexes, undergoes continuous degradation and do not explode on heating [21,34,85,86]. A significant common feature shared by the three pNb compounds, *viz.*, **NbAla (4.1)**, **NbVal (4.2)** and **KNb** as evident from the respective thermograms, is the absence of water molecule in the compounds whereas **NbA (4.3)** and **NbN (4.4)** showed dehydration degradation for water of crystallization. In the case of the neat tetraperoxoniobate complex, **KNb**, (**Fig. 4.20**) the degradation associated with peroxide loss occurs in the temperature range of 165-255 °C with the weight loss of 18.3% where the temperature range is close to the reported value for the complex **NaNb** [6]. The corresponding thermogravimetric analysis data for the developed pNb compounds are presented in **Table 4.5**.

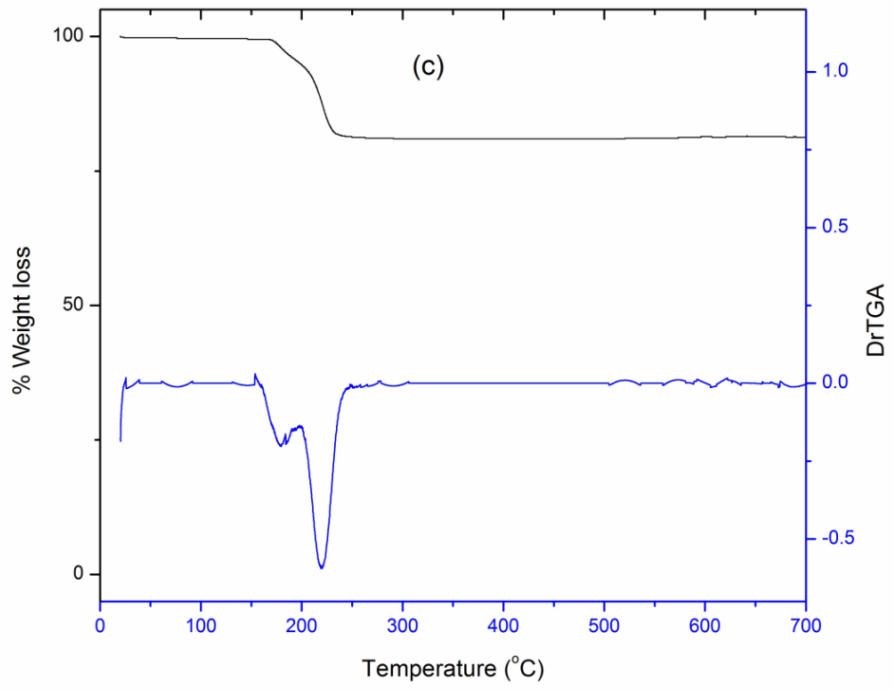

Fig. 4.20 TGA-DTG plot of **KNb**.

The first decomposition stage occurs in **NbAal** (**4.1**) (**Fig. 4.21**) and **NbVal (4.2)** (**Fig. 4.22**) in the temperature ranges of 135-210 °C with the corresponding weight loss of 21.7% and 140-205 °C with the equivalent weight loss of 24.9%, respectively,

attributable to loss of co-ordinated peroxo groups from the complexes. As the observed weight loss is slightly less than the expected value, it is likely that part of the oxygen is retained with niobium to form oxoniobium species, as has been observed previously in case of neat as well as heteroligand pNb complexes [21,34,85,86]. Subsequently, ligand degradation takes place in the temperature range of 243-480 °C in case of **NbAla (4.1)** [241-389 °C for **NbVal** (**4.2**)] and further continues up to a final decomposition temperature of 700 °C. The total weight loss which occurred during the overall decomposition process was evaluated to be 33.4% in case of **NbAla (4.1)** and 40.6% in case of **NbVal (4.2)** for the loss of the components *viz.,* co-ordinated peroxide and the co-ligand, assuming that four of the ligand oxygen atoms are being retained to form the oxoniobate species as the final degradation product.

Although existence of homo- or heteroleptic pNb complexes without free or bound water molecule is not unprecedented [1,21,31,61,62], the majority of heteroligand pNb complexes and sodium tetraperoxoniobate, **NaNb** [6] contain either outer sphere or co-ordinated, or both types of water molecules [1,21,31,34]. The first stage of decomposition for **NbA (4.3)** (**Fig 4.23**) occurs in the temperature range of 78-102 ^{o}C, with the liberation of the lattice water from the complex. The corresponding weight loss of 8.9% is in good agreement with the value of 8.1% calculated for two molecules of water of crystallization. The next decomposition stage is in the temperature range of 157-189 ^{o}C attributable to loss of peroxo groups from the complexes with weight loss of 18.8%. Similarly, here also the observed weight loss is slightly less than the expected value which has been discussed in the thermal degradation of **NbAla (4.1)** and **NbVal (4.2)**. A further increase in temperature leads to continuous degradation of the arginine ligand up to a final decomposition temperature of 700°C. The total weight loss which occurred during the overall decomposition process was evaluated to be 54.3%, which agrees well with the theoretically calculated value of 54.6%, for the loss of the components *viz.,* water molecule, co-ordinated peroxide and the co-ligand, assuming that four of the ligand oxygen atoms are being retained to form the oxoniobate species as the final degradation product.

It is notable that the thermogram for **NbN (4.4)** (**Fig. 4.24**) displayed two step dehydration process in the temperature range of 45-105°C, providing conclusive evidence for the presence of outer sphere as well as co-ordinated water molecules in the

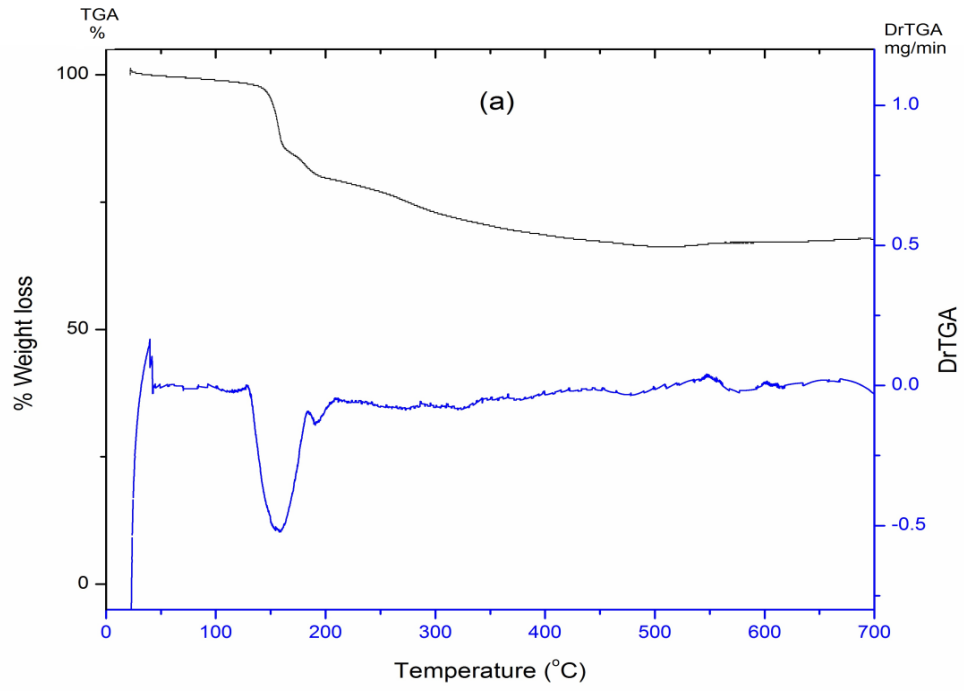

Fig. 4.21 TGA-DTG plot of **NbAla**.

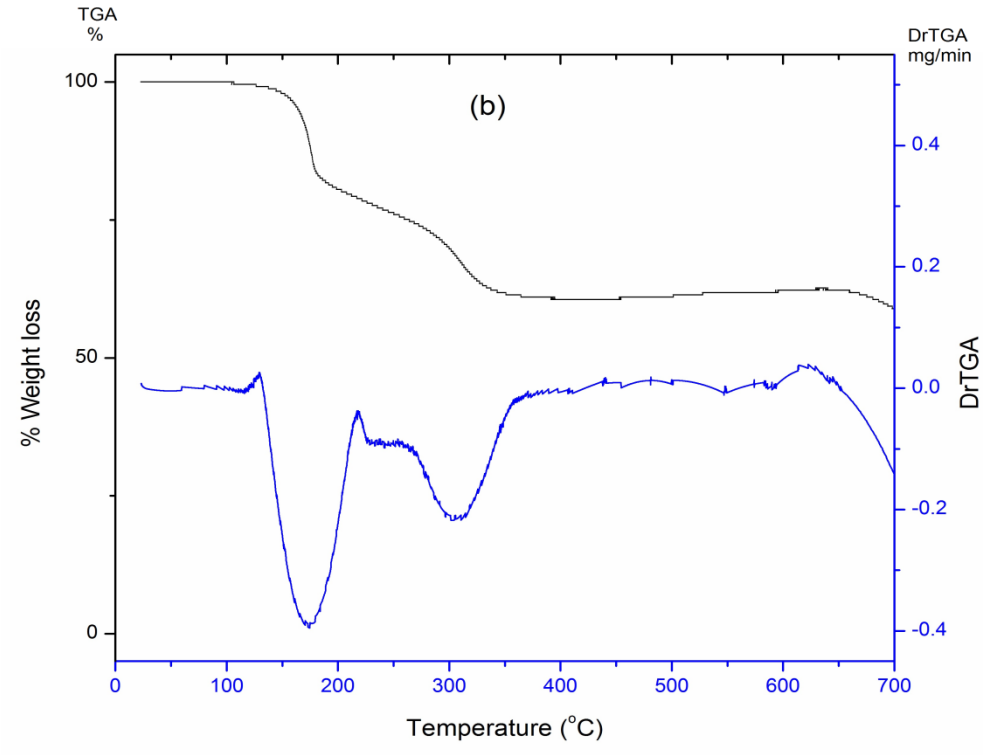

Fig. 4.22 TGA-DTG plot of **NbVal**.

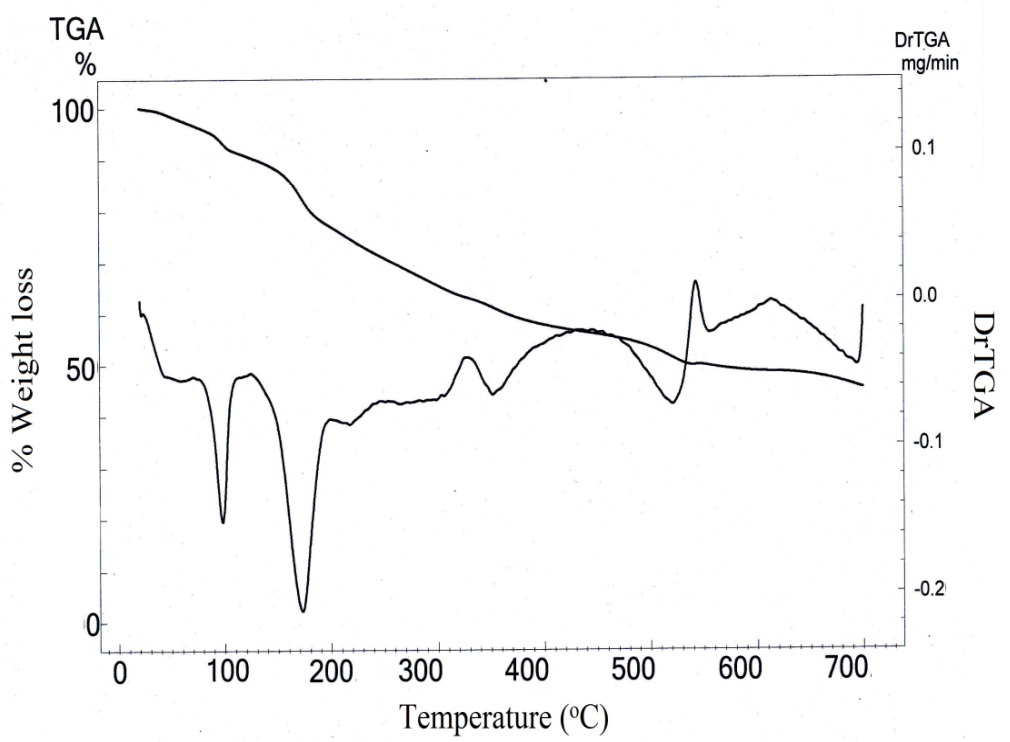

Fig. 4.23 TGA-DTG plot of **NbA**.

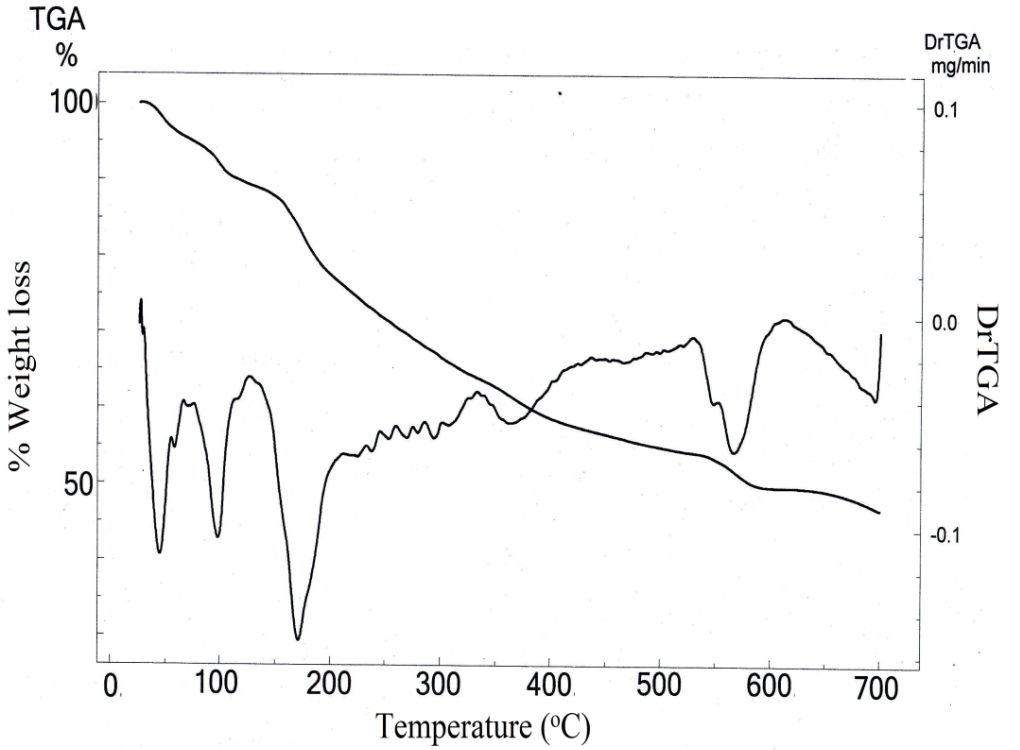

Fig. 4.24 TGA-DTG plot of **NbN**.

compound, consistent with the formula assigned. The decomposition step occurring at relatively higher temperature between 90 to 105 °C, after the initial liberation of the outer sphere water molecule in the temperature range of 45-70 ^{o}C, is attributable to the loss of the co-ordinated water molecule. The observed total weight loss of 9.8% corresponding to the two steps combined, is close to the calculated value of 9.2% for the release of two molecules of water from the complex. After the dehydration, the thermal behaviour of catalysts **NbA (4.3)** and **NbN (4.4)** are quite similar. The compound **NbN (4.4)** undergoes continuous degradation with loss of peroxide in the temperature range of 158-189 °C analogous to compound **4.3**, followed by the loss of the nicotinic acid ligand up to the final temperature of 700 °C.

The residue remaining from the pNb compounds after their complete degradation was characterized to be oxoniobate species. The IR spectrum of the residue showed the characteristic *ν*(Nb=O) absorptions and complete disappearance of the signature peaks pertaining to peroxo as well as amino acids of the original compounds. The TGA-DTG analysis data for the compounds thus furnished further endorsement in support of the composition and formula assigned to the compounds.

Table 4.5 Thermogravimetric data of peroxoniobium compounds, **KNb** and **4.1**-**4.4**

Compound	Temperature range (°C)	Observed weight loss (%)	Final residue (%)
KNb	165-255	18.34	81.66
NbAla	135-210	21.73	66.21
	243-480	12.06	
NbVal	140-205	24.88	59.37
	241-389	15.75	
NbA	78-102	8.9	45.56
	157-189	18.8	
	245-700	26.74	
NbN	45-70	4.44	47.03
	90-105	5.41	
	158-189	16.55	
	250-700	26.57	

Taking into account the above collective evidence, the structure of the complex ions may be represented by eight co-ordinated polyhedra of the type shown in **Fig. 4.25**, comprising of three terminal peroxo groups and an amino acid occurring as a bidentate ligand, bonded to Nb(V) *via* carboxylate and amino groups. The structure of **NbN** includes nicotinate anion occurring as a unidentate ligand bonded to the Nb centre through the carboxylate group, the side-on bound peroxo groups and a co-ordinated water molecule completing eight-fold co-ordination around Nb.

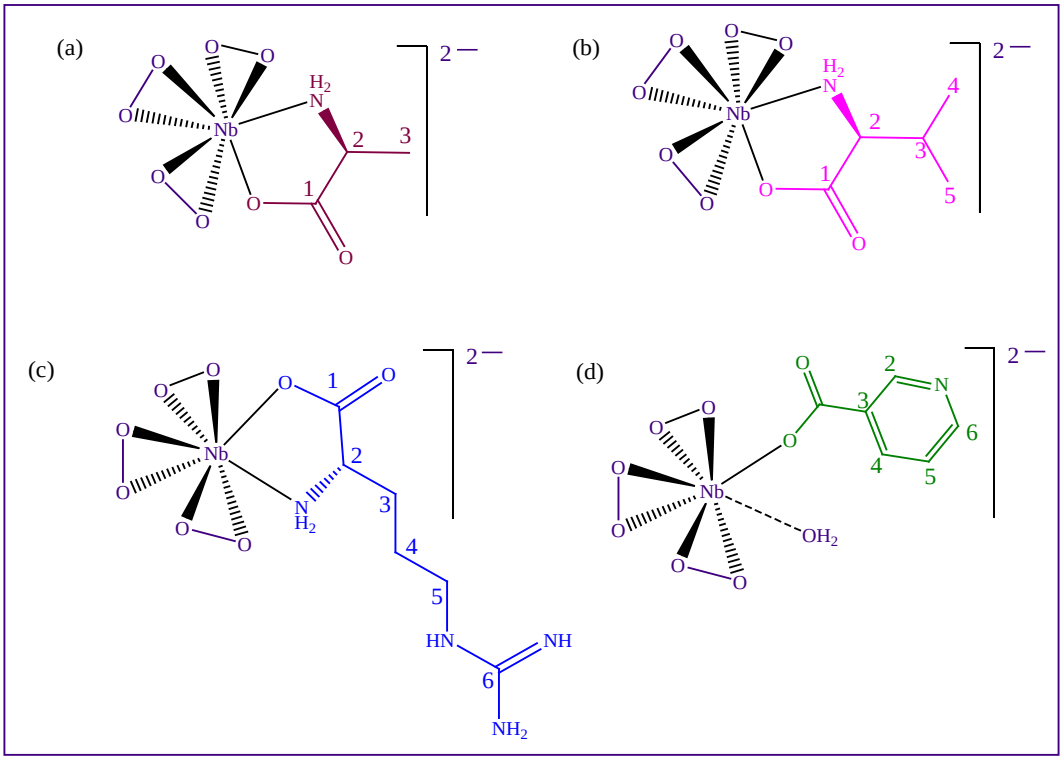

Fig. 4.25 Proposed structure of (a) **NbAla (4.1)**, (b) **NbVal (4.2)**, (c) **NbA (4.3)** and (d) **NbN (4.4)**.

4.3.2.4 Theoretical investigation

The viability of the proposed structures for the complexes **4.1-4.4** was further supported by the results of density functional theory (DFT) [60] calculations at the B3LYP/LANL2DZ level of theory. The initial structures of the complexes were modelled on the basis of the experimentally derived structural information. Presented in **Fig. 4.26** are the optimized geometries of the niobium complexes which show coordination spheres of the two complexes comprising of central metal atom (Nb)

surrounded by three η^2-peroxo groups and deprotonated amino acid ligand bonded *via* O(carboxylate) and N(amino) atoms. While one of the peroxo groups occupies a *trans* position to the co-ligand, the other two are in *cis* configuration. The coordination polyhedron around the niobium atom in each of the complexes is a dodecahedron which is in accord with the structures of majority of the reported pNb complexes [1,34]. Moreover, the geometrical parameters such as the bond angles and bond lengths obtained from DFT calculations (**Table 4.6)** are within the range typical of the heteroleptic peroxoniobium(V) complexes. The bond distances associated with the peroxo groups *viz.*, Nb-O and O-O bonds vary between 2.023 to 2.086 Å and 1.552 to 1.557 Å, respectively. The geometrical parameters derived from the theoretical calculations are in close agreement with the reported crystallographic data obtained for other triperoxoniobium(V) complexes consisting of N,O-donor ligands in the co-ordination sphere [1,31,32,34].

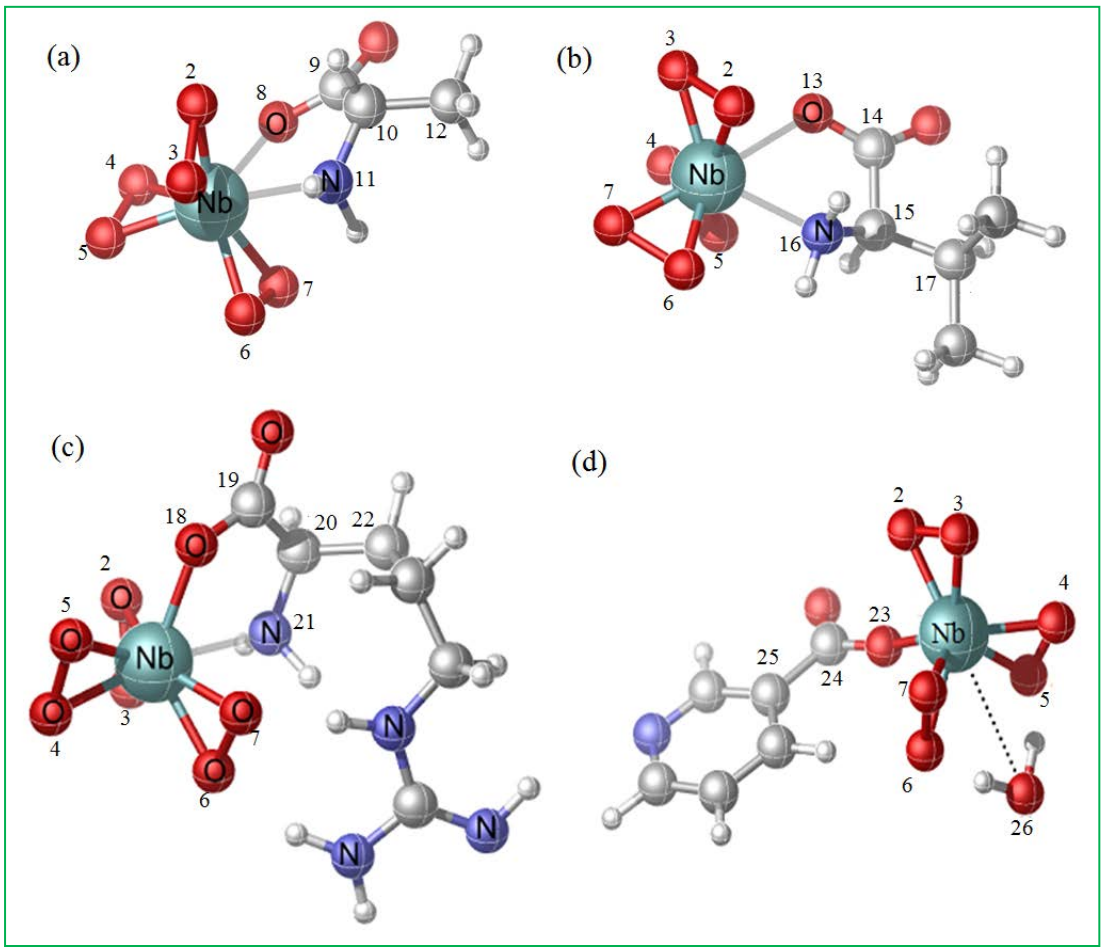

Fig. 4.26 Optimized geometry of (a) **NbAla (4.1)**, (b) **NbVal (4.2)**, (c) **NbA (4.3)** and (d) **NbN (4.4)**. The numerical numbers represent the labeling of the atoms as in **Table 4.6**.

Table 4.6 Selected bond lengths (in Å) and bond angles (in degree) for the pNb complexes calculated at B3LYP/LANL2DZ level of theory

Structural index[a]	**NbAla**	Structural index[a]	**NbVal**	Structural index[a]	**NbA**	Structural index[a]	**NbN**
Nb-O2	2.062	Nb-O2	2.042	Nb-O2	2.072	Nb-O2	2.047
Nb-O3	2.059	Nb-O3	2.038	Nb-O3	2.008	Nb-O3	1.999
Nb-O4	2.029	Nb-O4	2.032	Nb-O4	1.999	Nb-O4	1.977
Nb-O5	2.024	Nb-O5	2.041	Nb-O5	2.066	Nb-O5	2.033
Nb-O6	2.042	Nb-O6	2.076	Nb-O6	2.011	Nb-O6	1.985
Nb-O7	2.086	Nb-O7	2.023	Nb-O7	2.086	Nb-O7	2.040
Nb-O8	2.225	Nb-O13	2.392	Nb-O18	2.162	Nb-O23	2.138
O2-O3	1.552	O2-O3	1.553	O2-O3	1.526	O2-O3	1.527
O4-O5	1.557	O4-O5	1.556	O4-O5	1.533	O4-O5	1.530
O6-O7	1.549	O6-O7	1.547	O6-O7	1.530	O6-O7	1.532
C9-O8	1.310	C14-O13	1.295	C19-O18	1.307		
C10-C12	1.542	C14-C15	1.551	C20-C22	1.537	C24-C25	1.521
Nb-N11	2.394	Nb-N16	2.331	Nb-N21	2.370	Nb-O26	2.831
∠O2-Nb-O3	44.01	∠O2-Nb-O3	43.01	∠O2-Nb-O3	43.9	∠O2-Nb-O3	44.3
∠O4-Nb-O5	45.18	∠O4-Nb-O5	44.58	∠O4-Nb-O5	44.9	∠O4-Nb-O7	44.8
∠O6-Nb-O7	44.26	∠O6-Nb-O7	44.75	∠O6-Nb-O7	44.2	∠O5-Nb-O6	44.7
∠O8-Nb-N11	70.32	∠O13-Nb-N16	66.94	∠O8-Nb-N11	72.1	∠O23-Nb-O26	82.9

[a]See **Fig. 4.26** for atomic numbering.

We have also calculated vibrational frequencies for the optimized geometries of the studied pNb compounds. The theoretically obtained IR and Raman data presented in **Table 4.2,** correlated well with the respective experimentally determined frequencies. The small deviations observed between the calculated and experimental spectral data appear to be within the acceptable limit and are not unusual as the calculated spectral data were obtained from gas phase optimized geometries of the complexes. The reported average error for frequencies calculated with the B3LYP functional was of the order 40-50 cm^{-1} for inorganic molecules [87]. Thus the results of our theoretical studies substantiate the experimental observations and impart additional validity to the proposed geometries for the developed pNb complexes.

4.3.2.5 Crystal structure of KNb

The crystallographic parameters for the structure of **KNb** are summarized in **Table 4.7** and the selected bond lengths and bond angles are listed in **Table 4.8**. The single crystal X-ray analysis revealed that niobium is coordinated with four peroxo groups in the inner sphere of the complex $K_3[Nb(O_2)_4]$ with three potassium counter cations in the outer sphere balancing the charge on the anionic complex species (**Fig. 4.27**). The potassium cation connects $[Nb(O_2)_4]^{3-}$ units through peroxo oxygen. Interestingly, the crystal packing of **KNb** has been observed to be different from **NaNb** (**Table 4.7**).

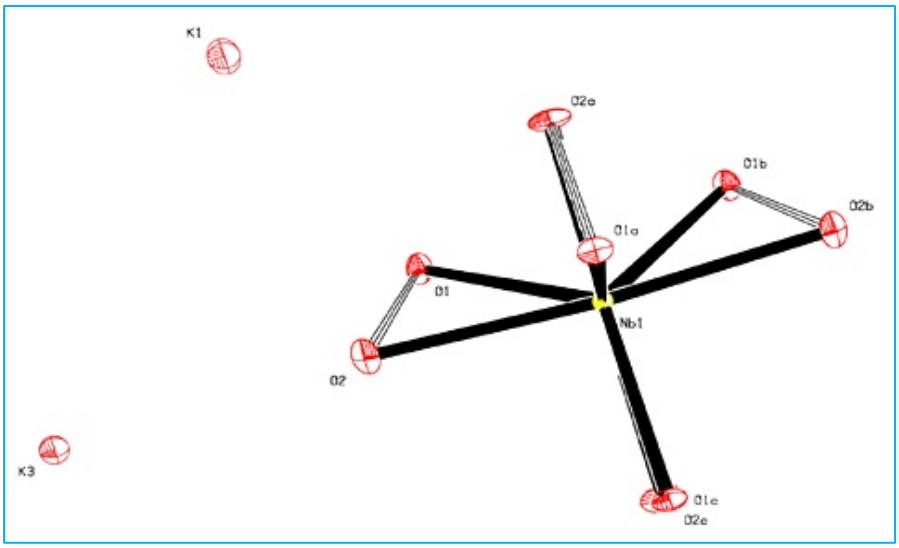

Fig. 4.27 ORTEP of **KNb** with 50% probability ellipsoid [asymmetric unit]

The peroxo unit connects Nb and K cation providing the closed packed structure for **KNb**. Each oxygen atom from peroxo unit is linked to one Nb and three K^+ cations showing a rigid environment that holds the conformation of $[Nb(O_2)_4]^{3-}$. On the other hand, in case of **NaNb**, the Na^+ ions are surrounded by six water molecules as has been reported elsewhere [6]. There is no direct interaction between the Na^+ cations and the $[Nb(O_2)_4]^{3-}$ anions. Thus the overall structure is less rigid for **NaNb** compared to **KNb**.

Table 4.7 Crystallographic data of $K_3[Nb(O_2)_4]$ (**KNb**), compared with reported Sodium tetraperoxoniobate $Na_3[Nb(O_2)_4]\cdot 13H_20$ (**NaNb**) [6]

Crystal Data	**KNb**	**NaNb**
Formula unit	K_3NbO_8	$Na_3NbO_{21}H_2$ 6
Formula wt.	338.21	523.91
Crystal system	Tetragonal	Triclinic
T [K]	100	193
a [Å]	6.7850(2)	7.6449
b [Å]	6.7850(2)	8.7726
c [Å]	7.7718(3)	9.1643
α [°]	90	64.103
β [°]	90	81.83
γ [°]	90	69.80
Volume [Å^3]	357.78(2)	518.85
Space group	$I4_2/m$	P-1
Z	2	1
D_{calc} [g cm^{-3}]	3.139	1.735
μ/mm^{-1}	3.432	-
Reflns. Collected	3301	-
Unique reflns.	3246	-
Observed reflns.	255	-
R_1 [I>2σ(I)], wR_2	0.0274; 0.0677	0.043, 0.105
GOF	1.429	-
Instrument	Bruker APEX-II	STOE-IPDS
X-ray	MoK\α; λ=0.71073	MoK\α; λ=0.71073
CCDC Reference No./Code	1426204	

Table 4.8 Description of crystal data

Atomic coordinates

Atom	X/a	Y/b	Z/c
Nb1	0.50000(0)	0.50000(0)	0.50000(0)
O1	0.35969(31)	0.35969(31)	0.30895(39)
O2	0.28684(29)	0.28684(29)	0.47939(59)
K1	0.00000(0)	0.50000(0)	0.25000(0)
K3	0.00000(0)	0.00000(0)	0.50000(0)

Bond distances (Angstrom)

Nb1 - O1	2.0043(27)
Nb1 - O2	2.0516(20)
O1 - O2	1.4978(50)
O1 - K1	2.6594(21)
O2 - K1	3.0096(31)
O2 - K3	2.7570(20)
K1 - K3	3.9095(1)

Bond angles (deg)

O1 - Nb1 - O2	43.32(0.09)
Nb1 - O1 - O2	70.02(0.15)
Nb1 - O1 - K1	113.17(0.10)
O2 - O1 - K1	88.15(0.13)
Nb1 - O2 - O1	66.66(0.12)
Nb1 - O2 - K1	99.40(0.08)
Nb1 - O2 - K3	172.19(0.10)
O1 - O2 - K1	62.03(0.12)
O1 - O2 - K3	121.15(0.14)
K1 - O2 - K3	85.25(0.06)
O1 - K1 - O2	29.83(0.06)
O1 - K1 - K3	66.66(0.05)
O2 - K1 - K3	44.65(0.04)
O2 - K3 - K1	50.10(0.04)

Torsion angles (deg)

O2	-Nb1	-O1	-K1	78.87(0.16)
O1	-Nb1	-O2	-K1	-53.89(0.13)
O1	-Nb1	-O2	-K3	180.00(1.20)
Nb1	-O1	-O2	-K1	115.51(0.09)
Nb1	-O1	-O2	-K3	180.00(0.19)
K1	-O1	-O2	-Nb1	-115.51(0.09)
K1	-O1	-O2	-K3	64.49(0.17)
Nb1	-O1	-K1	-O2	-67.31(0.16)
Nb1	-O1	-K1	-K3	-103.70(0.11)
O2	-O1	-K1	-K3	-36.39(0.14)
Nb1	-O2	-K1	-O1	57.13(0.14)
Nb1	-O2	-K1	-K3	-173.68(0.16)
O1	-O2	-K1	-K3	129.19(0.18)
K3	-O2	-K1	-O1	-129.19(0.18)
Nb1	-O2	-K3	-K1	126.89(1.14)
O1	-O2	-K3	-K1	-53.11(0.19)
O1	-K1	-K3	-O2	24.83(0.10)

4.4 Conclusion

The present work afforded a series of water soluble pNb complexes which contain species familiar to those found in biological environment as co-ligand. The spectral and chemical data obtained have provided satisfactory evidence for the composition of the ligand sphere in each of the complexes and the likely mode of ligation to the Nb(V) centre, which has been corroborated by the results of DFT calculations performed on the complexes. Moreover, the crystal structure of homoleptic $K_3[Nb(O_2)_4]$ has been determined.

The work presented in Chapters 6-7 demonstrates that the title complexes are stable in solution and exhibit biologically important properties. The results of our study on catalytic activity of the complexes in organic oxidation are described in Chapter 5.

References

1. Bayot, D. and Devillers, M. Peroxo complexes of niobium(V) and tantalum(V). *Coordination Chemistry Reviews*, 250(19):2610-2626, 2006.
2. Stavber, G., Malič, B., and Kosec, M. A road to environmentally friendly materials chemistry: low-temperature synthesis of nanosized $K_{0.5}Na_{0.5}NbO_3$ powders through peroxide intermediates in water. *Green Chemistry*, 13(5):1303-1310, 2011.
3. Leite, E. R., Vila, C., Bettini, J., and Longo, E. Synthesis of niobia nanocrystals with controlled morphology. *The Journal of Physical Chemistry B*, 110(37):18088-18090, 2006.
4. Egami, H. and Katsuki, T. Nb(salan)-catalyzed asymmetric epoxidation of allylic alcohols with hydrogen peroxide. *Angewandte Chemie International Edition*, 47(28):5171-5174, 2008.
5. Egami, H., Oguma, T., and Katsuki, T. Oxidation catalysis of Nb(salan) complexes: asymmetric epoxidation of allylic alcohols using aqueous hydrogen peroxide as an oxidant. *Journal of the American Chemical Society*, 132(16):5886-5895, 2010.
6. Passoni, L. C., Siddiqui, M. R. H., Steiner, A., and Kozhevnikov, I. V. Niobium peroxo compounds as catalysts for liquid-phase oxidation with hydrogen peroxide. *Journal of Molecular Catalysis A: Chemical*, 153(1):103-108, 2000.
7. Maniatakou, A., Karaliota, S., Mavri, M., Raptopoulou, C., Terzis, A., and Karaliota, A. Synthesis, characterization and crystal structure of novel mononuclear peroxotungsten(VI) complexes. Insulinomimetic activity of W(VI) and Nb(V) peroxo complexes. *Journal of Inorganic Biochemistry*, 103(5):859-868, 2009.
8. Thomadaki, H., Lymberopoulou-Karaliota, A., Maniatakou, A., and Scorilas, A. Synthesis, spectroscopic study and anticancer activity of a water-soluble Nb(V) peroxo complex. *Journal of Inorganic Biochemistry*, 105(2):155-163, 2011.
9. Conte V. and Di Furia, F. In Strukul, G., editor, *Catalytic Oxidations with Hydrogen Peroxide as Oxidant*, page 223. Kluwer Academic Publishers, The Netherlands, 1992.
10. Conte, V., Di Furia, F., and Moro, S. The chemistry of peroxovanadium species in aqueous solutions. Structure and reactivity of a neutral diperoxovanadium complex as provided by ^{51}V-NMR data, ab initio calculations and kinetic results. *Journal of Molecular Catalysis A: Chemical*, 120(1-3):93-99, 1997.

11. Conte, V., Di Furia, F., and Moro, S. Peroxovanadium complexes as radical oxidants in organic solvents and in aqueous solutions. *Journal of Molecular Catalysis A: Chemical*, 117(1-3):139-149, 1997.
12. Mimoun, H., Saussine, L., Daire, E., Postel, M., Fischer, J., and Weiss, R. Vanadium(V) peroxy complexes. New versatile biomimetic reagents for epoxidation of olefins and hydroxylation of alkanes and aromatic hydrocarbons. *Journal of the American Chemical Society*, 105(10):3101-3110, 1983.
13. Vuletić, N. and Djordjević, C. Co-ordination complexes of niobium and tantalum XVII. Diperoxotetrafluoro-niobates(V) and tantalates(V). *Journal of the Less Common Metals*, 45(1):85-89, 1976.
14. Geetha, R., Rao, P. S., Babu, V., and Subramanian, S. EPR and structural investigations on single crystals of $K_2NbO_2F_5 \cdot H_2O$. *Inorganic Chemistry*, 30(7):1630-1635, 1991.
15. Stomberg, R. The crystal-structure of sodium pentafluoroperoxoniobate(V) monohydrate, $Na_2[NbF_5(O_2)].H_2O$. *Acta Chemica Scandinavica Series A-Physical and Inorganic Chemistry*, 34(3):193-198, 1980.
16. Stomberg, R. The crystal structure of sodium pentafluoroperoxoniobate(V) dihydrate, $Na_2[NbF_5(O_2)] \cdot 2H_2O$, *Acta Chemica Scandinavica A*,35(7):489-495, 1981.
17. Stomberg, R. The crystal structure of trisodium pentafluoroperoxoniobate(V) hydrogendiflouride, $Na_3[HF_2][NbF_5(O2)]$, *Acta Chemica Scandinavica A*, 35(6):389-394, 1981.
18. Stomberg, R. The crystal structure of 1,10-phenanthrolinium pentafluoroperoxoniobate(V), $(C_{12}H_{10}N_2)[NbF_5(O_2)]$, *Acta Chemica Scandinavica A*, 36(1):101-108, 1982.
19. Stomberg, R. The disordered structure of bis (8-hydroxyquinolinium) pentafluoroperoxoniobate(V) trihydrate, $(C_9H_8NO)_2[NbF_5(0_2)] \cdot 3H_20$. A redetermination at. *Acta Chemica Scandinavica A*, 37(6):523-530, 1983.
20. Djordjevic, C. and Vuletic, N. Coordination complexes of niobium and tantalum. V. Eight-coordinated di- and triperoxoniobates(V) and -tantalates(V) with some nitrogen and oxygen bidentate ligands. *Inorganic Chemistry*, 7(9):1864-1868, 1968.
21. Bayot, D., Tinant, B., and Devillers, M. Water-soluble niobium peroxo complexes as precursors for the preparation of Nb-based oxide catalysts. *Catalysis Today*, 78(1):439-447, 2003.

22. Vuletic, N., Prcić, E., and Djordjevic, C. Co-ordination complexes of niobium and tantalum. XVIII. Peroxo-EDTA niobates(V) and tantalates(V). *Zeitschrift für Anorganische und Allgemeine Chemie*, 450(1):67-69, 1979.
23. Narendar, Y. and Messing, G. L. Synthesis, decomposition and crystallization characteristics of peroxo− citrato− niobium: an aqueous niobium precursor. *Chemistry of Materials*, 9(2):580-587, 1997.
24. Vin, T. F., Tarakanova, A. V., Kostyuchenko, O. V., Tarasevich, B. N., Kulikov, N. S., and Anisimov, A. V. Oxidation of organosulfur compounds by hydrogen peroxide in the presence of niobium and vanadium peroxo complexes. *Theoretical Foundations of Chemical Engineering*, 42(5):636-642, 2008.
25. Deschamps, P., Kulkarni, P. P., and Sarkar, B. The crystal structure of a novel copper(II) complex with asymmetric ligand derived from L-histidine. *Inorganic Chemistry*, 42(23):7366-7368, 2003.
26. Sarkar, B. Treatment of Wilson and Menkes diseases. *Chemical Reviews*, 99(9):2535-2544, 1999.
27. DiDonato, M. and Sarkar, B. Copper transport and its alterations in Menkes and Wilson diseases. *Biochimica et Biophysica Acta (BBA)-Molecular Basis of Disease*, 1360(1):3-16, 1997.
28. Christodoulou, J., Danks, D. M., Sarkar, B., Baerlocher, K. E., Casey, R., Horn, N., Tümer, Z., and Clarke, J. T. Early treatment of Menkes disease with parenteral Cooper-Histidine: Long-term follow-up of four treated patients. *American Journal of Medical Genetics Part A*, 76(2):154-164, 1998.
29. Sorenson, J. R. J. In Berthon, G., editor, *Handbook of Metal-Ligand Interactions in Biological Fluids: Bioinorganic Medicine*, pages 2:1128-1139. Marcel Dekker: New York, 1995.
30. Messai, A., Benali-Cherif, R., Jeanneau, E., and Benali-Cherif, N. trans-Diaquabis (dl-valinato-κ^2N,O)nickel(II). *Acta Crystallographica Section E: Structure Reports Online*, 67(9):m1204-m1204, 2011.
31. Bayot, D., Tinant, B., Mathieu, B., Declercq, J. P., and Devillers, M. Spectroscopic and structural characterizations of novel water-soluble peroxo [polyaminocarboxylatobis(N-oxido)]niobate(V) complexes. *European Journal of Inorganic Chemistry*, 2003(4):737-743, 2003.

32. Bayot, D., Tinant, B., and Devillers, M. Homo-and heterobimetallic niobium V and tantalum V peroxo-tartrate complexes and their use as molecular precursors for Nb-Ta mixed oxides. *Inorganic Chemistry*, 44(5):1554-1562, 2005.
33. Bayot, D., Degand, M., Tinant, B., and Devillers, M. Spectroscopic and structural characterizations of water-soluble peroxo complexes of niobium(V) with N-containing heterocyclic ligands. *Inorganica Chimica Acta*, 359(5):1390-1394, 2006.
34. Maniatakou, A., Makedonas, C., Mitsopoulou, C. A., Raptopoulou, C., Rizopoulou, I., Terzis, A., and Karaliota, A. Synthesis, structural and DFT studies of a peroxo-niobate complex of the biological ligand 2-quinaldic acid. *Polyhedron*, 27(16):3398-3408, 2008.
35. Gad, M. Z. Anti-aging effects of L-arginine. *Journal of Advanced Research*, 1(3):169-177, 2010.
36. Cotton, F. A., Hazen Jr., E. E. In Boyer P. D., editor, *The Enzymes*, volume IV. Academic Press, New York, 1971.
37. Girasolo, M. A., Rubino, S., Portanova, P., Calvaruso, G., Ruisi, G., and Stocco, G. New organotin(IV) complexes with l-Arginine, Nα-t-Boc-l-Arginine and l-Alanyl-l-Arginine: Synthesis, structural investigations and cytotoxic activity. *Journal of Organometallic Chemistry*, 695(4):609-618, 2010.
38. Cylwik, D., Mogielnicki, A., and Buczko, W. L-arginine and cardiovascular system. *Pharmacological Reports*, 57(1):14-22, 2005.
39. Köse, D. A., Toprak, E., Avcı, E., Avcı, G. A., Şahin, O., and Büyükgüngör, O. Synthesis, spectral, thermal studies of Co(II), Ni(II), Cu(II) and Zn(II)-arginato complexes. Crystal structure of monoaquabis(arginato-κO,κN) copper(II). $[Cu(arg)_2(H_2O)]\cdot NaNO_3$. *Journal of the Chinese Chemical Society*, 61(8):881-890, 2014.
40. Nazir, M. and Naqvi, I. I. Synthesis, spectral and electrochemical studies of complex of uranium(IV) with pyridine-3-carboxylic acid. *American Journal of Analytical Chemistry*, 4(3): 134-140, 2013.
41. Shara, M., Kincaid, A. E., Limpach, A. L., Sandstrom, R., Barrett, L., Norton, N., Bramble, J. D., Yasmin, T., Tran, J., Chatterjee, A., and Bagchi, M. Long-term safety evaluation of a novel oxygen-coordinated niacin-bound chromium(III) complex. *Journal of Inorganic Biochemistry*, 101(7):1059-1069, 2007.
42. Shara, M., Yasmin, T., Kincaid, A. E., Limpach, A. L., Bartz, J., Brenneman, K. A., Chatterjee, A., Bagchi, M., Stohs, S. J., and Bagchi, D. Safety and toxicological

evaluation of a novel niacin-bound chromium(III) complex. *Journal of Inorganic Biochemistry*, 99(11):2161-2183, 2005.

43. Jensen, N. L. *U.S. Patent No. 4,923,855*. Washington, DC: U.S. Patent and Trademark Office, 1990.
44. Szymańska, A., Nitek, W., Mucha, D., Karcz, R., Pamin, K., Połtowicz, J., and Łasocha, W. Structural studies and physico-chemical properties of new oxodiperoxomolybdenum complexes with nicotinic acid. *Polyhedron*, 60:39-46, 2013.
45. Sarmah, S., Kalita, D., Hazarika, P., Borah, R., and Islam, N. S. Synthesis of newer dinuclear and mononuclear peroxo-vanadium(V) complexes containing biogenic co-ligands: A comparative study of some of their properties, *Polyhedron*, 23:1097-1107, 2004.
46. Sarmah, S., Hazarika, P., Islam, N. S., Rao, A. V. S., and Ramasarma, T. Peroxo-bridged divanadate as a selective bromide oxidant in bromoperoxidation, *Molecular and Cellular Biochemistry*, 236:95-105, 2002.
47. Sarmah, S. and Islam, N. S. A dinuclear peroxo-vanadium(V) complex with coordinated tripeptide. Synthesis, spectra and reactivity in bromoperoxidation. *Journal of Chemical Research*, 2001(5):172-174, 2001.
48. Djordjevic, C., Vuletic, N., Renslo, M. L., Puryear, B. C., and Alimard, R. Peroxo heteroligand vanadates(V): Synthesis, spectra-structure relationships, and stability toward decomposition. *Molecular and Cellular Biochemistry*, 153(1):25-29, 1995.
49. Kalita, D., Deka, R. C., and Islam, N. S. Density functional studies on structure and reactivity of a dinuclear peroxovanadate(V) complex. *Inorganic Chemistry Communications*, 10(1):45-48, 2007.
50. Hazarika, P., Sarmah, S., Kalita, D., and Islam, N. S. New peroxovanadium compounds containing biogenic co-ligands: synthesis, stability and effect on alkaline phosphatase activity. *Transition Metal Chemistry*, 33(1):69-77, 2008.
51. Kalita, D., Das, S. P., and Islam, N. S. Kinetics of inhibition of rabbit intestine alkaline phosphatase by heteroligand peroxo complexes of vanadium(V) and tungsten(VI). *Biological Trace Element Research*, 128(3):200-219, 2009.
52. Haldar, A. K., Banerjee, S., Naskar, K., Kalita, D., Islam, N. S., and Roy, S. Sub-optimal dose of sodium antimony gluconate (SAG)-diperoxovanadate combination clears organ parasites from BALB/c mice infected with antimony resistant

Leishmania donovani by expanding antileishmanial T-cell repertoire and increasing IFN-γ to IL-10 ratio. *Experimental Parasitology*, 122(2):145-154, 2009.

53. Khanna, V., Jain, M., Barthwal, M. K., Kalita, D., Boruah, J. J., Das, S. P., Islam, N. S., Ramasarma, T. and Dikshit, M. Vasomodulatory effect of novel peroxovanadate compounds on rat aorta: Role of rho kinase and nitric oxide/cGMP pathway. *Pharmacological Research*, 64(3):274-282, 2011.
54. Djordjevic, C., Vuletic, N., Jacobs, B. A., Lee-Renslo, M., and Sinn, E. Molybdenum(VI) peroxo α-amino acid complexes: synthesis, spectra, and properties of $MoO(O_2)_2$(α-aa)(H_2O) for α-aa= glycine, alanine, proline, valine, leucine, serine, asparagine, glutamine, and glutamic acid. X-ray crystal structures of the glycine, alanine, and proline compounds. *Inorganic Chemistry*, 36(9):1798-1805, 1997.
55. Hazarika, P., Kalita, D., Sarmah, S., Borah, R., and Islam, N. S. New oxo-bridged dinuclear peroxotungsten(VI) complexes: Synthesis, stability and activity in bromoperoxidation. *Polyhedron*, 25(18):3501-3508, 2006.
56. Hazarika, P., Kalita, D., Sarmah, S., and Islam, N. S. New oxo-bridged peroxotungsten complexes containing biogenic co-ligand as potent inhibitors of alkaline phosphatase activity. *Molecular and Cellular Biochemistry*, 284(1):39-47, 2006.
57. Hazarika, P., Kalita, D., and Islam, N. S. Mononuclear and dinuclear peroxotungsten complexes with co-ordinated dipeptides as potent inhibitors of alkaline phosphatase activity. *Journal of Enzyme Inhibition and Medicinal Chemistry*, 23(4):504-513, 2008.
58. Djordjevic, C., Puryear, B. C., Vuletic, N., Abelt, C. J., and Sheffield, S. J. Preparation, spectroscopic properties, and characterization of novel peroxo complexes of vanadium(V) and molybdenum(VI) with nicotinic acid and nicotinic acid N-oxide. *Inorganic Chemistry*, 27(17):2926-2932, 1988.
59. Frisch, M. C., *et al.*, Gaussian 09, Revision A.1, Gaussian, Inc., Wallingford, CT, 2009; Gaussian 09, Revision A.1, M. J. Frisch, G. W. Trucks, H. B. Schlegel, G. E. Scuseria, M. A. Robb, J. R. Cheeseman, G. Scalmani, V. Barone, B. Mennucci, G. A. Petersson, H. Nakatsuji, M. Caricato, X. Li, H. P. Hratchian, A. F. Izmaylov, J. Bloino, G. Zheng, J. L. Sonnenberg, M. Hada, M. Ehara, K. Toyota, R. Fukuda, J. Hasegawa, M. Ishida, T. Nakajima, Y. Honda, O. Kitao, H. Nakai, T. Vreven, J. A. Montgomery Jr., J. E. Peralta, F. Ogliaro, M. Bearpark, J. J. Heyd, E. Brothers, K. N.

Kudin, V. N. Staroverov, R. Kobayashi, J. Normand, K. Raghavachari, A. Rendell, J. C. Burant, S. S. Iyengar, J. Tomasi, M. Cossi, N. Rega, J. M. Millam, M. Klene, J. E. Knox, J. B. Cross, V. Bakken, C. Adamo, J. Jaramillo, R. Gomperts, R. E. Stratmann, O. Yazyev, A. J. Austin, R. Cammi, C. Pomelli, J. W. Ochterski, R. L. Martin, K. Morokuma, V. G. Zakrzewski, G. A. Voth, P. Salvador, J. J. Dannenberg, S. Dapprich, A. D. Daniels, O. Farkas, J. B. Foresman, J. V. Ortiz, J. Cioslowski and D. J. Fox, Gaussian, Inc., Wallingford CT, 2009.

60. Parr R. G. and Yang, W. *Density Functional Theory of Atoms and Molecules*. Oxford University Press, Oxford, 1989.
61. Balke, C. W. and Smith, E. F. Observations on columbium. *Journal of the American Chemical Society*, 30(11):1637-1668, 1908.
62. Cage, B., Weekley, A., Brunel, L. C., and Dalal, N. S. K_3CrO_8 in K_3NbO_8 as a proposed standard for g-factor, spin concentration, and field calibration in high-field EPR spectroscopy. *Analytical Chemistry*, 71(10):1951-1957, 1999.
63. Titova V. A. and Slatinskaya, I. G. Potassium and sodium peroxyorthoniobates, *Zhurnal Neorganicheskoi Khimii,* 14(12):3283-3285, 1969.
64. Bayot, D., Devillers, M., and Peeters, D. Vibrational spectra of eight-coordinate niobium and tantalum complexes with peroxo ligands: A theoretical simulation. *European Journal of Inorganic Chemistry*, 2005(20):4118-4123, 2005.
65. Griffith, W. P. 1005. Studies on transition-metal peroxy-complexes. Part III. Peroxy-complexes of groups IV A, VA, and VI A. *Journal of the Chemical Society (Resumed)*, 5248-5253, 1964.
66. Nakamoto, K. *Infrared and Raman Spectra of Inorganic and Co-ordination Compounds, Part B.* Wiley and Sons, New York, 62-67, 1997.
67. Deacon, G. B. and Phillips, R. J. Relationships between the carbon-oxygen stretching frequencies of carboxylato complexes and the type of carboxylate coordination. *Coordination Chemistry Reviews*, 33(3):227-250, 1980.
68. De Gelder, J., De Gussem, K., Vandenabeele, P., and Moens, L. Reference database of Raman spectra of biological molecules. *Journal of Raman Spectroscopy*, 38(9):1133-1147, 2007.
69. Nazir, M. and Naqvi, I. I. Synthesis, spectral and electrochemical studies of complex of uranium(IV) with pyridine-3-carboxylic acid. *American Journal of Analytical Chemistry*, 4(03):134-140, 2013.

70. Kumar, M. and Yadav, R. A. Experimental IR and Raman spectra and quantum chemical studies of molecular structures, conformers and vibrational characteristics of nicotinic acid and its N-oxide. *Spectrochimica Acta Part A: Molecular and Biomolecular Spectroscopy*, 79(5):1316-1325, 2011.
71. Dilip, C. S., Venkatachalam, K. J., Raj, A. P., and Ramachandramoorthy, T. Microwave assisted synthesis and structural characterisation of nicotinic acid and nitrito–κO mixed ligand complexes. *Life*, 50:L80-L88, 2011.
72. Chang, J. C., Gerdom, L. E., Baenziger, N. C., and Goff, H. M. Synthesis and molecular structure determination of carboxyl bound nicotinic acid (niacin) complexes of chromium(III). *Inorganic Chemistry*, 22(12):1739-1744, 1983.
73. Chow, S. T. and Mcauliffe, C. A. Complexes of amino acids and derivatives-XIII some Nickel(II) complexes of L-arginine zwitterions or L-argininate anions. A novel ionic → bidenetate perchlorate rearangement brought about by pressure [1-5]. *Journal of Inorganic and Nuclear Chemistry*, 37(4):1059-1064, 1975.
74. Kumar, S. and Rai, S. B. Spectroscopic studies of L-arginine molecule, *Indian journal of Pure and Applied Physics*, 48:251-255, 2010.
75. Viera, I., Torre, M. H., Piro, O. E., Castellano, E. E., and Baran, E. J. Structural and spectroscopic characterization of aqua-diargininate-copper(II)-carbonate monohydrate. *Journal of Inorganic Biochemistry*, 99(5):1250-1254, 2005.
76. Nakamoto, K. *Infrared and Raman Spectra of Inorganic and Co-ordination Compounds, Part B.* Wiley and Sons, New York, 55, 1997.
77. Nath, M., Yadav, R., Eng, G., and Musingarimi, P. Characteristic spectral studies and *in vitro* Antimicrobial and *in vivo* multi-infection antifungal activities in mice of new organotin(IV) derivatives of heterocyclic amino acids. *Applied Organometallic Chemistry*, 13(1):29-37, 1999.
78. Ratilla, E. M. A., Scott, B. K., Moxness, M. S., and Kostic, N. M. Terminal and new bridging coordination of methylguanidine, arginine, and canavanine to platinum(II). The first crystallographic study of bonding between a transition metal and a guanidine ligand. *Inorganic Chemistry; (USA)*, 29(5):918-926, 1990.
79. Khan, T., Halle, J. C., Simonnin, M. P., and Schaal, R. Hydrogen-1 and carbon-13 nuclear magnetic resonance investigation of nicotinic acid, its anion, and cation, in water and water-dimethyl sulfoxide mixtures. Influence of dimethyl sulfoxide on relative acidities. *The Journal of Physical Chemistry*, 81(6):587-590, 1977.

80. Bayot, D., Tinant, B., and Devillers, M. Spectroscopic and structural characterizations of ammonium peroxo-carboxylato molybdate(VI) complexes. *Inorganica Chimica Acta*, 357(3):809-816, 2004.
81. Luí, M., Caldeira, M. M., and Gil, V. M. NMR spectroscopy study of the peroxovanadium(V) complexes of L-malic acid. *Inorganica Chimica Acta*, 356:179-186, 2003.
82. Dengel, A. C., Griffith, W. P., Powell, R. D., and Skapski, A. C. Studies on transition-metal peroxo complexes. Part 7. Molybdenum(VI) and tungsten(VI) carboxylato peroxo complexes, and the X-ray crystal structure of $K_2[MoO(O_2)_2(glyc)]\cdot 2H_2O$. *Journal of the Chemical Society, Dalton Transactions*, (5):991-995, 1987.
83. Boruah, J. J., Kalita, D., Das, S. P., Paul, S., and Islam, N. S. Polymer-anchored peroxo compounds of vanadium(V) and molybdenum(VI): synthesis, stability, and their activities with alkaline phosphatase and catalase. *Inorganic Chemistry*, 50(17):8046-8062, 2011.
84. Boruah, J. J., Das, S. P., Ankireddy, S. R., Gogoi, S. R., and Islam, N. S. Merrifield resin supported peroxomolybdenum(VI) compounds: recoverable heterogeneous catalysts for the efficient, selective and mild oxidation of organic sulfides with H_2O_2. *Green Chemistry*, 15(10):2944-2959, 2013.
85. Ghosh, J. K. and Jere, G. V. Kinetics of solid state decomposition of $K_3[Nb(O_2)_4]$ and $K_3[Ta(O_2)_4]$: A thermogravimetric study. *Thermochimica Acta*, 136:73-80, 1988.
86. Jere, G. V., Surendra, L., and Gupta, M. K. Solid state decomposition studies on tetraperoxo species of transition metals. Kinetics of the isothermal decomposition of $K_3Nb(O2)_4$ and $K_3Ta(O_2)_4$. *Thermochimica Acta*, 63(2):229-236, 1983.
87. Bytheway, I. and Wong, M. W. The prediction of vibrational frequencies of inorganic molecules using density functional theory. *Chemical Physics Letters*, 282(3):219-226, 1998.